Modelling, Simulation and Control of a Novel Structure Varying Quadrotor

Moad Idrissi[a*], Mohammad Salami[a], Fawaz Annaz[a]

[a]*Faculty of Computing, Engineering and the Built Environment, Birmingham City University, Birmingham, United Kingdom.*

Abstract

In this work, a novel structure of a Quadrotor Unmanned Aerial Vehicle (UAV) is proposed to change the dynamics during flight. The proposed mechanism is presented which consists of extendable plates that move along the horizontal axes from the body frame respectively. Essentially, the main goal behind this novel architecture is to enhance performance and improve flight duration in reaching the desired position. The Euler dynamic model is derived to represent the multirotor equation of motion. Basic PID controllers were implemented to demonstrate the concept and to analyse the vehicle behaviour as the structure is altered during flight. A physical modelling software is also used to study the multi-body interactions of rigid bodies as well as the dynamic response. By comparing the performance between the proposed system and the traditional version, the paper reveals improved flight performance for attitude and position tracking. The mathematical representation of the dynamic system was also verified using Msc ADAMS as identical control inputs where simultaneously applied.

*Corresponding author.
E-mail address:* moad.idrissi@mail.bcu.ac.uk

1. Introduction

Recently, UAVs have received an enormous interest due to their missions carried out successfully by the operator. In particular, vertical take-off and landing (VTOL) vehicles are becoming more popular due to their orientation capabilities, which makes them suitable for various applications such as surveillance, indoor flying, rescue missions, delivery and many more [1]. As there are various UAVs available in the literature, Quadrotors have emerged to be the most popular VTOL systems. The mechanical structure is known to accumulate more advantages over other types of VTOLs such as less power consumption, fair stability in case of motor failure, ease of development and maintenance [2].

With regards to Quadrotors, great research has been undertaken to study and analyse the functionality, where the mathematical model creates a theoretical environment of the dynamics using advanced simulation tools such as Simulink. Additional control algorithms are then applied by which the UAV can respond according to the users desired input (e.g. attitude or position tracking). For instance, the authors in [3] have used the Euler approach to describe the dynamics of a Quadrotor where the six degrees of freedom (6-DOF) can be viewed. A flight controller is then designed with a main objective of guaranteeing the state variables to converge to the reference values in finite time. Other authors in [4] have also

presented the full equations of motion for a Quadrotor while considering the gyroscopic effects from the propeller, rotational torques and the drag forces due to air resistance. Control techniques are designed to achieve a promising performance from the system before the practical experiments are initiated [5].

Although there is a great research undertaken regarding VTOL UAVs, many researchers have proposed innovative approaches into improving the performance of these vehicles. Majority of which have modified controllers to meet the user requirement[5–7], while others have modified the mechanical structure [8–10].

Since this research proposes a novel structure, there is currently a great research implemented into the tilting mechanism where authors have clearly improved the performance. However, other drawbacks are also introduced such as increased power consumption, increased actuation requirement, structural complexities and increased mass [11]. Additionally, this may increase the risk of flight failure while a mission is carried out due to the additional actuators used for the tilting mechanism. For instance, the authors in [12] who have recently proposed the novel tilt rotor mechanism to move along narrower routes have mentioned that future work will be focused on improving the energy consumption and developing a fail-safe strategy if any of the actuators fail. Tilt-wing UAVs have also received a lot of interest from researchers. They consists of two wings that are initially placed in a vertical direction, two actuators are generally connected to the edge of each wing, facing vertically upwards. When the vehicle reaches a reasonable altitude, the wings can transition from a vertical position to a horizontal position in order to achieve the horizontal take-off and landing (HTOL) performance [13, 14, 16].

The Tail-sitter has recently emerged as a hybrid UAV that can vertically take off and land on its tail. It also has the ability to achieve HTOL performance by transitioning the complete body as the speed of particular actuators are increased. In comparison to the tilt-rotor and tilt-wing quadrotors, the tail-sitters consists of more benefits due to its ability of transitioning without the need of any extra actuators, making the design mechanically simpler with less weight to carry [8, 11, 15]. However, the risk of wing stalling, vulnerability against cross winds and the complexity of mathematical modelling and control is greatly increased [15,16].

Although significant research is currently undertaken to improve the functionality of these novel configurations. Other structural modification have been carried out to meet the requirements of certain applications, such as arm manipulators [17], single grippers [18] or using the whole quadrotor body to pick up various objects [19]. As for the Tilt-rotors, Tilt-wing and Tail-sitters, these have become widely researched due to their capabilities of achieving a hybrid performance [8, 12, 13]. Although these UAVs consist of more advantages due to structural changes [14, 15, 16], conventional Quadrotors are still continuously rising in demand due to their ease of development, mechanically simpler to understand, and the availability of various sizes has made them suitable for many applications [20,21]. However, it is believed that very little research has been undertaken to improve the flight performance by modifying the structure while maintaining the characteristics of the conventional version.

So far, Siddhardha, K. has attempted to achieve attitude motions by adjusting the mechanical structure during flight. Essentially, four retractable landing gears that consist of payloads are attached to each end of the Quadrotor chassis. DC motor are then used to retract the landing gear during flight which causes the attitude to change in the relative direction. The author mentions that the performance of the vehicle is very limited but can be implemented following extensive research and further studies [22]. The proposed novel structure is in fact unique and ideally realisable, however, numerous limitations and drawbacks are presented such as increased mass, costs, structural complexities and lacks controllability where we believe that it is problematical to develop or design the system based on the study presented.

On the other hand, representing the dynamic behaviour of a Quadrotor is monumentally expressed as a set of mathematical equations that characterises the vehicles full degrees of freedom. However, un-modelled factors and uncertainties may reduce the accuracy of the simulation in comparison to the experimental study. For instance, UAVs that have multi body interactions such as the tilting mechanism lacks the theoretical description of the aerodynamic effects, which results in the accuracy of the model being further reduced [23].

In this paper, we propose a novel Quadrotor platform that consists of an interchangeable chassis in order to improve the flight performance. The work will focus on using a physical modelling software to accurately assess the dynamic behaviour. This approach will not only provide accurate data of the vehicle dynamics, but will also justify the equations of motion for this novel study where a comparison between the results attained from the equation of motions will be

compared against the physical modelling software. Last but not least, PID controllers are designed and implemented on the Quadrotor model in order to verify the performance capabilities and to ensure that stability is achievable.

The paper is organised as followed: the proposed contribution is presented in section 2 followed by discussing the novel mechanical structure in section 3. Next, sections 4 entails the method of mathematically representing the dynamics of a novel Quadrotor as compared to the traditional version. Section 5 consists of designing and implementing the PID controller while section 6 and 7 verifies the performance using Simulink and ADAMS environment.

2. Problem Formulation

The concept of proposing the novel structure is to improve the flight performance of a traditional Quadrotor throughout the mission criteria. The objective of this approach is to ensure that the attitude as well as the position tracking is improved, where the desired states can be reached. Essentially, the study will focus on creating a novel mechanism that consists of minimum limitations and drawbacks by ensuring that the final design consists of similar characteristics to the conventional version.

Since the multirotor heavily relies on angular rotations to achieve motion, the chassis will be adapted in order to predominantly effect the vehicles attitude. Hence, the body will be split into three mechanical components that can interchange to fluctuate the centre of mass during flight. The extendable plates are configured to move along horizontal directions with respect to the quadrotor shell in order to affect the vehicles dynamics. These extensions are achieved by setting

the desired position using PID control techniques where an acceleration is generated. The proposed assessments will consist of changing the structure during hovering conditions, rotational angles and while reaching the desired position.

To simulate these behaviours, the mathematical representation is derived and modelled using the common approach; Simulink. However, the anticipated mechanical system consists of multi body interactions, which becomes difficult to mathematically model as the accuracy is reduced. Therefore, verifying the performance will be relied on a physical modelling simulator that is capable of accurately demonstrating the kinematics and dynamics of the proposed geometry. This research will focus on using Msc ADAMS due to its intensive capability of presenting the dynamics of almost any computer aided design (CAD) geometry, making it one of the most popular software within the engineering field [22]. A comparative study between the mathematical model and the physical model will be carried out based on selecting identical system parameters. This is achieved by ensuring that ADAMS geometry designed on SolidWorks to consist of similar characteristics to the proposed mathematical model.

3. Proposed System Structure

Initially, physical components and parameters such as the actuators, propellers and the vehicle chassis must be designed and calculated accordingly in order to carry out a comparison between both software. The overall mass of the vehicle is considered to contain the accumulation of all the component masses. Hence, a simpler geometry is developed such that the modified chassis can be easier to analyse and study.

It is worth mentioning that the proposed system designed on SolidWorks provides a key advantage of analysing the contact behaviour and the interaction between two bodies. Essentially, the criteria of attaching the extendable plates to the Quadrotor shell must be uniquely formed in order to attain similar characteristics to the traditional version, preventing the exposure of any new limitations to the overall system. Therefore, the vehicle is modified accordingly to consist of unfilled areas in order to attain identical performance to the traditional Quadrotor. Figure 1 illustrates an overview of the chassis where it can be seen that there are two hollow regions. To ensure that both plates extend whenever necessary, the shell has been uniquely formed to enable the retraction of individual plates without effecting one another.

a) Quadrotor shell (Hallow region)   b) Quadrotor shell with plates (Top view)

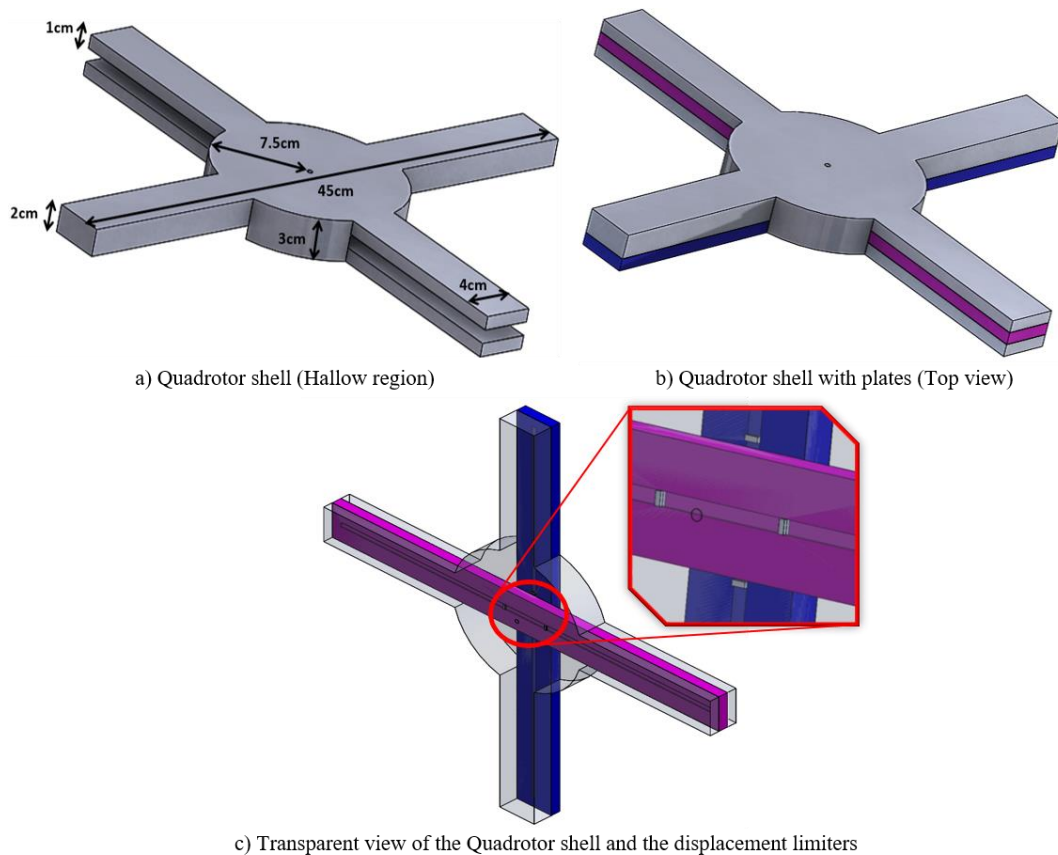c) Transparent view of the Quadrotor shell and the displacement limiters

Figure 1. Novel geometry designed using SolidWorks (isometric view).

With regards to the operation of the extendable plates, it is assumed that a stepper motor is used to generate the sliding displacement. For simplicity, a force is purely applied to the plates, causing the sliding motion to occur along the relative direction. However, the quick orientation capabilities of the Quadrotor carries a risk of the extendable plates to excessively slide out during angular rotations, causing the stability to become negatively affected. Hence, the designed prototype consists of mechanical blocks that are relatively placed in series along each extendable plate in an effort to limit the displacement from both directions as shown on figure 1 (c).

It is worth mentioning that both plates are designed using the exact same dimensions and will also contain the same material, mass and moment of inertia (MOI). This approach ensures that the response of the vehicle is equivalent as the plate is respectively displaced. For instance, extending one plate that carries more mass than the other plate will cause the UAV to present a different trend in response while increasing the complexity of analysis.

Finally, combining all of the geometric components creates the final prototype of the proposed model as shown in figure 2. Two opposite motors are using the same clockwise (CW) propeller configuration while the other two use the same counter clockwise (CCW) propellers. This ensures that the aerodynamics generated is accordingly distributed, where the vehicle can achieve successful lift without introducing unwanted drifts. With regards to the translational displacement of each plate, a limit has been set to 15cm along each direction in order to maintain stability throughout the analysis for this prototype. The displacement of extendable plate 1 (EP1) is set to move along the y-axis of the

body frame while the displacement of extendable plate 2 (EP2) will move along the x-axis.
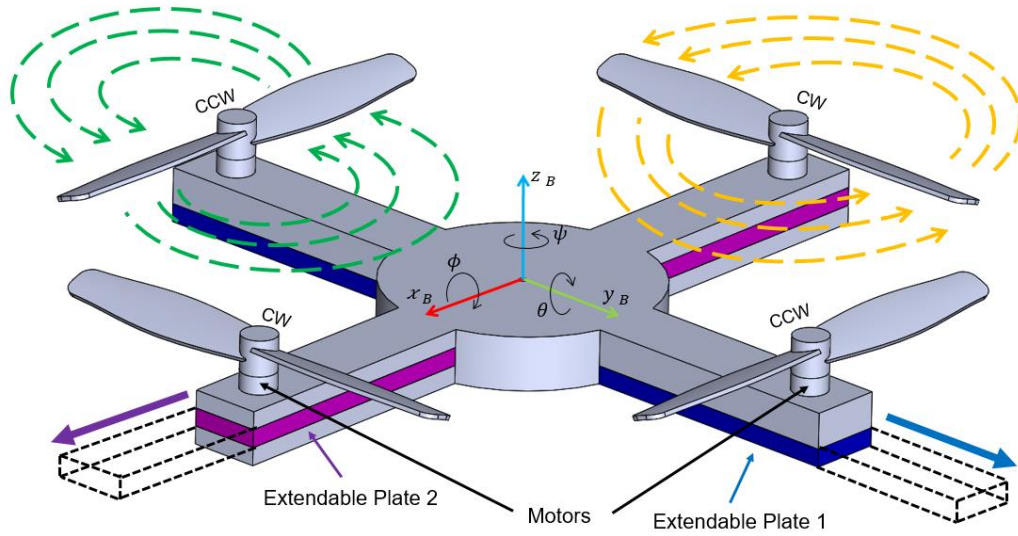

Figure 2. Proposed Quadrotor model with an interchangeable chassis.

4. Dynamic Modelling of the Proposed System

The mathematical model assumes that all the components are rigid and are symmetrically structured; All four propellers and motors are of the same manufacturer and are all equivalent in size. Without any plate extension, the length between each motor to the centre of mass are all equivalent, and that the thrust generated by each motor is faced vertically upward from the body.

4.1. Flight Operation

Figure 3 illustrates the selected Quadrotor which consists of four actuators placed 90° apart similar to a '+' configuration. Motor 1 and 3 are set to rotate in the CW direction while motor 2 and 4 rotate in the CCW direction, which are referred to $Set_{1,3}|_{cw}$ and $Set_{2,4}|_{ccw}$. Since the Quadrotor is an under-actuated mechanical system that possesses less control inputs than the 6-DOF. Figure 3 (a)

illustrates that simultaneously increasing the speeds of all the motors will enforce the UAV to purely lift in the vertical direction. Hence, all arrows facing upwards have an equivalent height which represents the speed of the relative motor. Achieving a roll angle is shown on figure 3 (b) where the angular velocity of motor 2 is set higher than motor 4, and the angular velocity for $Set_{1,3}|_{cw}$ is kept constant. Similarly, increasing the angular velocity of motor 3 in comparison to motor 1 while maintaining $Set_{2,4}|_{ccw}$ constant will incur a pitching angle as shown on figure 3 (c). Finally, achieving a yaw motion is presented in figure 3 (d) where the angular velocity of two opposite motors will simultaneously increase while the remaining motors are simultaneously reduced.
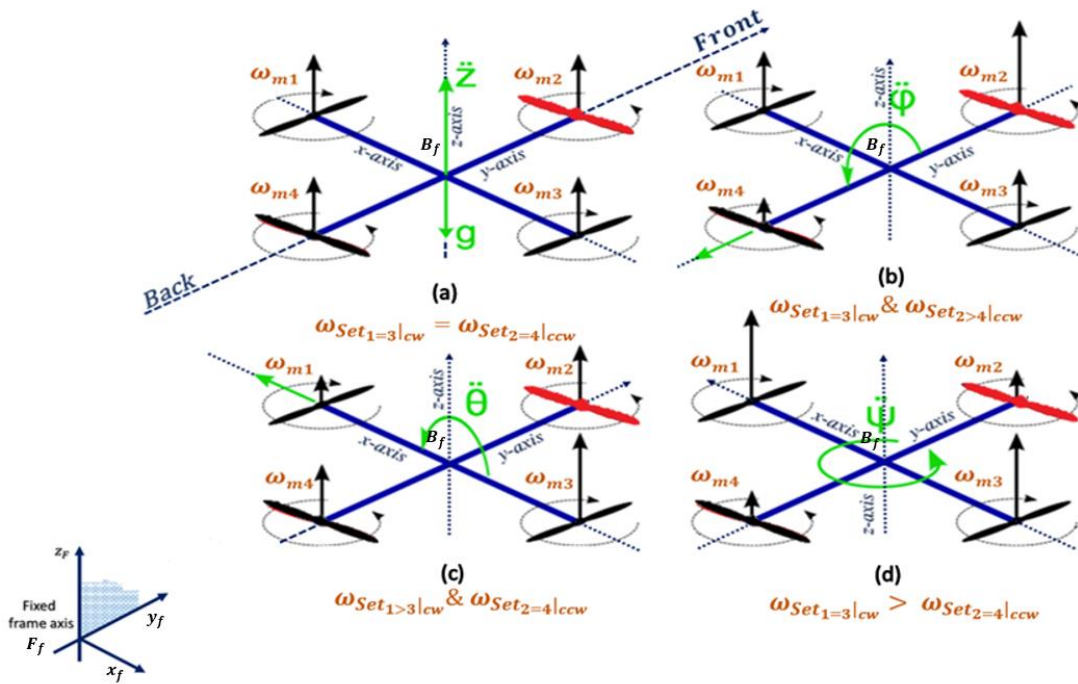

Figure 3. Quadrotor operation for lift, rolling, pitching and yawing.

Once a thrust is generated, the displacement is measured with respect to the inertial frame of reference or 'fixed frame axis' on figure 3. In other words,

identifying the location of the Quadrotor in mathematical terms is essentially described as the correlations between two coordinate frames [24].

- Fixed frame axis (F_f) – An earth fixed coordinate system with the origin located on the ground.

$$F_F = (x_F, y_F, z_F)$$

- Body frame axis (B_f) – The origin coordinate system located on the vehicles centre of gravity.

$$F_b = (x, y_B, z_B)$$

In summary of the operation and the relationship between the motions of the vehicle and the coordinate frame, table 1 presents the commands required for each rotation and the relative translational motion.

Command	$Set_{1,3}$	$Set_{2,4}$	Speed Status	Axis of Rotation	Axis of Motion
Hover (H)	$\omega_{m1} = \omega_{m3}$	$\omega_{m2} = \omega_{m4}$	$Set_{1,3} = Set_{2,4}$	N/A	$Z - axis$
CCW Pitch	$\omega_{m1} = \omega_{m3}$	$\omega_{m4} < \omega_{m2}$	N/A	$\sim Y - axis$	$\sim X - axis$
CCW Roll	$\omega_{m1} < \omega_{m3}$	$\omega_{m2} = \omega_{m4}$	N/A	$\sim X - axis$	$\sim Y - axis$
CCW Yaw	$\omega_{m1} = \omega_{m3}$	$\omega_{m2} = \omega_{m4}$	$Set_{1,3} > Set_{2,4}$	$\sim Z - axis$	N/A
CW Pitch	$\omega_{m1} = \omega_{m3}$	$\omega_{m4} > \omega_{m2}$	N/A	$Y - axis$	$X - axis$
CW Roll	$\omega_{m1} > \omega_{m3}$	$\omega_{m2} = \omega_{m4}$	N/A	$X - axis$	$Y - axis$
CW Yaw	$\omega_{m1} = \omega_{m3}$	$\omega_{m2} = \omega_{m4}$	$Set_{1,3} < Set_{2,4}$	$Z - axis$	N/A

Table 1. Rotational commands and axis of motion for a plus configured Quadrotor with respect to the inertial frame.

4.2. Conventional Quadrotor Modelling

Typically, the dynamic description of the UAV is defined by twelve states [25,26], which can be mathematically symbolised in x^T as shown in Equation (1):

$$x^T = \{x, \dot{x}, y, \dot{y}, z, \dot{z}, \phi, \dot{\phi}, \theta, \dot{\theta}, \psi, \dot{\psi})$$

(1)

Where $\{x, y, z, \dot{x}, \dot{y}, \dot{z}\}$ represents the respective positions and linear velocities, while $\{\phi, \theta, \psi, \dot{\phi}, \dot{\theta}, \dot{\psi}\}$ signifies the respective angular positions and velocities of rolling, pitching and yawing.

The orientations are mathematically described using Euler angles approach as shown on equation (2). The angles must be restricted to $-\frac{\pi}{2} \leq \phi, \theta \leq \frac{\pi}{2}$ and $-\pi \leq \psi \leq \pi$ in order to prevent singularities and maintain stability [27]. However, Numerous authors including those in [28] have further limited rolling and pitching angles to 0.35 radians (20°) to ensure a successful stability for the proposed UAV. Another researcher has also saturated the attitude angles to 0.2 radians (11.45°) in order to carry out a successful practical experiments with the Quadrotor [29], while others have restricted the angles to approximately 0.25 radians (15°) [30,31]. Moreover, the author in [32] has applied a disturbance on the Quadrotor where he mentions that the designed controller was able to tolerate the disturbance up to 0.52 radians (30°). Therefore, it has become customary for these limitations to be implemented in order to maintain an ideal performance especially during the early stages of experiment. As a result, the rotational limit for rolling and pitching in this study is set to $\theta_{lim} = \phi_{lim} = 0.6\, rad\, (Approx.\, 35°)$. The three elemental rotations is composed in the direct cosine matrix presented in equation (2) as [33]:

$$\mathbb{R}_M = \mathbb{R}_{(\psi,\theta,\phi\,)} = \begin{pmatrix} c_\psi c_\theta & c_\psi s_\theta s_\phi - c_\phi s_\psi & c_\phi s_\theta c_\psi + s_\psi s_\phi \\ c_\theta s_\psi & c_\psi c_\phi + s_\psi s_\theta s_\phi & s_\theta s_\psi c_\phi - c_\psi s_\phi \\ -s_\theta & c_\theta s_\phi & c_\theta c_\phi \end{pmatrix} \tag{2}$$

Where s and c denotes the respective sine and cosine. As the Quadrotor rotates in free space, a moment along the corresponding axis begins to generate a translational moment which is expressed by $\boldsymbol{r^{bf}}$ as [34]:

$$\boldsymbol{r^{bf}} = [x, y, z] \tag{3}$$

Expressing the MOI is represented by J^{bf} in equation (4) as [35]:

$$J^{bf} = \begin{pmatrix} I_{xx} & I_{xy} & I_{xz} \\ I_{xy} & I_{yy} & I_{yz} \\ I_{xz} & J_{yz} & I_{zz} \end{pmatrix} \tag{4}$$

Where J^{bf} contains scalar moments of inertia and the product of inertia. Assuming that the centre of mass is present and the body fixed axis are taken along principle axis of inertia, the sum of all moments about each axis is presented as [36]:

$$I_{xx}\ddot{\phi} + \dot{\theta}\dot{\psi}(I_{zz} - I_{yy}) = \tau_x \tag{5}$$

$$I_{yy}\ddot{\theta} + \dot{\phi}\dot{\psi}(I_{xx} - I_{zz}) = \tau_y \tag{6}$$

$$I_{zz}\ddot{\psi} + \dot{\phi}\dot{\theta}(I_{yy} - I_{xx}) = \tau_z \tag{7}$$

Where, τ_x, τ_y and τ_z represents the moment about each r^{bf} axis respectively and $\ddot{\phi}, \ddot{\theta}$ and $\ddot{\psi}$ represents the angular acceleration for rolling, pitching and yawing.

During flight, a gyroscopic torque is generated as a result of rolling and pitching. These rotational effects are theoretically expressed as [37,38]:

$$G_a = \sum_{i=1}^{4} J_r \, \dot{\omega} \Omega_i \tag{8}$$

Where J_r represents the moment of inertia, $\dot{\omega}$ is the angular velocity of the body frame and Ω_i is the angular rate of the rotor i ($i = 1, 2, 3, 4$).

Finding the total thrust generated by each actuator disk is derived using the propeller coefficients and squaring the motor speed as [39–41]:

$$\varsigma_i = K\Omega_i^2 \tag{9}$$

Where ς_i either represents the thrust or torque generated from the actuator disk according to K, which is a constant that represents the thrust factor b or the drag

factor d. These two coefficients are selected according to the orientation of the Quadrotor, where the thrust factor is considered during normal flight conditions except when the UAV is rotating about the z-axis (yaw) [42–44]:

$$b = C_T \rho D^4 \tag{10}$$
$$d = C_P \rho D^5 \tag{11}$$

Where C_T and C_P represents the thrust and power coefficient, ρ is the air density and D is the propeller diameter. These parameters are generally collected from the manufacturer's datasheet, where the propellers selected for this study are presented on table 2 [27].

Parameter Names	Symbol	Value
Diameter	D	$0.254\ m$
Thrust coefficient	C_T	0.121
Power Coefficient	C_P	0.0495
Air density	ρ	$1.255\ Kg/m^3$

Table 2. T-Style 10x5.5 propeller key parameter

Based on the parameters presented in table 2, the thrust and drag factor are calculated to:

$$b = C_T \rho D^4 = 6.317 \times 10^{-4} \tag{12}$$
$$d = C_P \rho D^5 = 1.61 \times 10^{-4} \tag{13}$$

Therefore, the input signals can be theoretically described as the addition and subtraction of the respective motor speeds in order to achieve the desired motion, which are expressed as [25]:

$$
\begin{cases}
U_1 = b\left(\Omega_1^2 + \Omega_2^2 + \Omega_3^2 + \Omega_4^2\right) \\
U_2 = b\left(\Omega_2^2 - \Omega_4^2\right) \\
U_3 = b\left(\Omega_3^2 - \Omega_1^2\right) \\
U_4 = d\left(\Omega_1^2 - \Omega_2^2 + \Omega_3^2 - \Omega_4^2\right)
\end{cases}
\tag{14}
$$

Where U_1 signifies the total thrust generated by the four actuator disks, U_2, U_3 and U_4 represent the total torque for rolling, pitching and yawing respectively. $\Omega_1, \Omega_2, \Omega_3$ and Ω_4 are defined as the angular velocity of each motors. Transposing the control inputs presented in Equation (14) to a matrix form is:

$$
\begin{bmatrix} U_1 \\ U_2 \\ U_3 \\ U_4 \end{bmatrix} =
\begin{bmatrix} b & b & b & b \\ 0 & b & 0 & -b \\ -b & 0 & b & 0 \\ d & -d & d & -d \end{bmatrix} *
\begin{bmatrix} \Omega_1^2 \\ \Omega_2^2 \\ \Omega_3^2 \\ \Omega_4^2 \end{bmatrix}
\tag{15}
$$

As for the gyroscopic effects about the x or y-axis, Equation (16) defines the residual angular velocity of the Quadrotor as Ω_r [45].

$$
\Omega_r = -\Omega_1 + \Omega_2 - \Omega_3 + \Omega_4
\tag{16}
$$

To obtain the full equations of motion, figure 4 illustrates the dynamic representation for the 6-DOF respectively, where system states such as acceleration, velocity, and position can be viewed once the integration process is carried out.

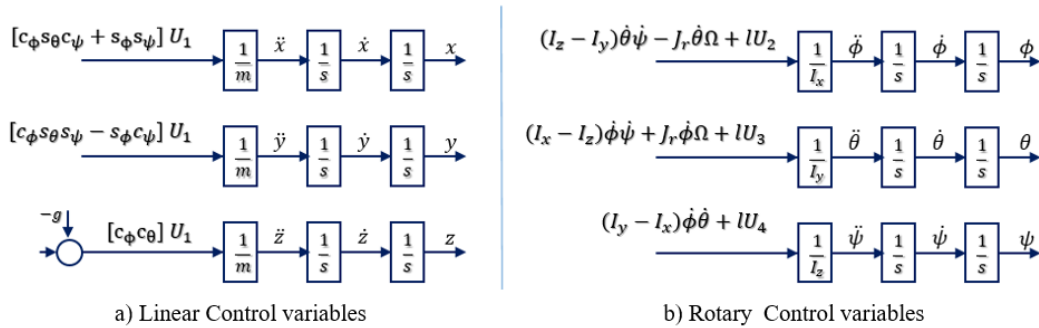a) Linear Control variables   b) Rotary Control variables

Figure 4. Integrating the vehicles dynamics.

Initially, the extendable plates are actively placed to match the behaviour of a traditional Quadrotor, where the centre of mass (COM) and MOI remain unchanged during the lifting procedure. Therefore, the mathematical model is obtainable through six set of equations as:

$$\ddot{x} = \frac{1}{m}[cos\phi sin\theta cos\psi + sin\phi sin\psi]\,U_1 \tag{17}$$

$$\ddot{y} = \frac{1}{m}[cos\phi sin\theta sin\psi - sin\phi cos\psi]\,U_1 \tag{18}$$

$$\ddot{z} = -g + \frac{1}{m}[cos\phi cos\theta]\,U_1 \tag{19}$$

$$\ddot{\phi} = \frac{1}{I_x}[\dot{\theta}\dot{\psi}(I_{zz} - I_{yy}) - J_r\dot{\theta}\Omega + lU_2] \tag{20}$$

$$\ddot{\theta} = \frac{1}{I_y}[\dot{\phi}\dot{\psi}(I_{xx} - I_{zz}) + J_r\dot{\phi}\Omega + lU_3] \tag{21}$$

$$\ddot{\psi} = \frac{1}{I_z}[\dot{\phi}\dot{\theta}(I_{yy} - I_{xx}) + U_4] \tag{22}$$

Where m denotes the total mass, g denotes the acceleration due to gravity and l represent the length from the motor to the centre of mass.

4.3. Novel Quadrotor Modelling

Since the novel structure is aimed at carrying minimised drawbacks similar to a traditional Quadrotor, it is believed that the mathematical representation is identical while the extendable plates are at their initial positions. However, any displacement of EP1 or EP2 will cause the vehicle COM to change accordingly. As a result, the MOI would also be effected as well as the quantity of torque required to rotate the vehicle. With regards to the equation of motion presented in equation (17) to (22), few changes must be applied such that the displacement of both extendable plates are respectively considered. While equation (17) to (19) purely focuses on the translational motion of the vehicle along each axis the constants that are effected are not considered within those equations, thus, they

remain untouched. As for equation (20) to (22), the constants; I_{zz}, I_{yy}, I_{xx} and l will become variables as EP1 and EP2 are displaced.

By considering the Quadrotor as a three dimensional figure, the masses are distributed in three dimensional space with mass component w_i at (y_i, x_i, z_i). The COM is a point vector notation (r_1, r_2, r_3) which is the position vector of w_1, w_2, w_3 with respect to the origin. Hence, the COM is a point whose position $\bar{r}$ is denoted as [46]:

$$\bar{r} = \frac{\sum w_i r_i}{\sum w_i} \tag{23}$$

For simplicity, three components are assigned masses; EP1, EP2 and the Quadrotor shell. In Figure 5, a two dimensional plane is presented which consists of pointing the COM at the centroid. Equation (24) and (25) expresses the approach used to determine the COM along each axis, where the Quadrotor shell has been split into two subcomponent in order to respectively analyse the behaviour during the extension of the relative plate.

$$\bar{r}_x = \frac{(w_2 \times (d_x + r_2)) + \left(\frac{w_3}{2} \times d_x\right)}{w_2 + \frac{w_3}{2}} \tag{24}$$

$$\bar{r}_y = \frac{(w_1 \times (d_y + r_1)) + (\frac{w_3}{2} \times d_y)}{w_1 + \frac{w_3}{2}} \tag{25}$$

Where $\bar{r}_x$ and $\bar{r}_y$ determines the COM point vector notation along the x and y-axis respectively, (w_1, w_2, w_3) signifies the mass of EP1, EP2 and the Quadrotor shell. d_x and d_y are constants that represent the initial COM measurements without any displacement of the plates. It is worth mentioning that the point vectors (r_1, r_2) are variables that are initially zero, which represents the initial positions of the extendable plate, and changes as they are displaced respectively.
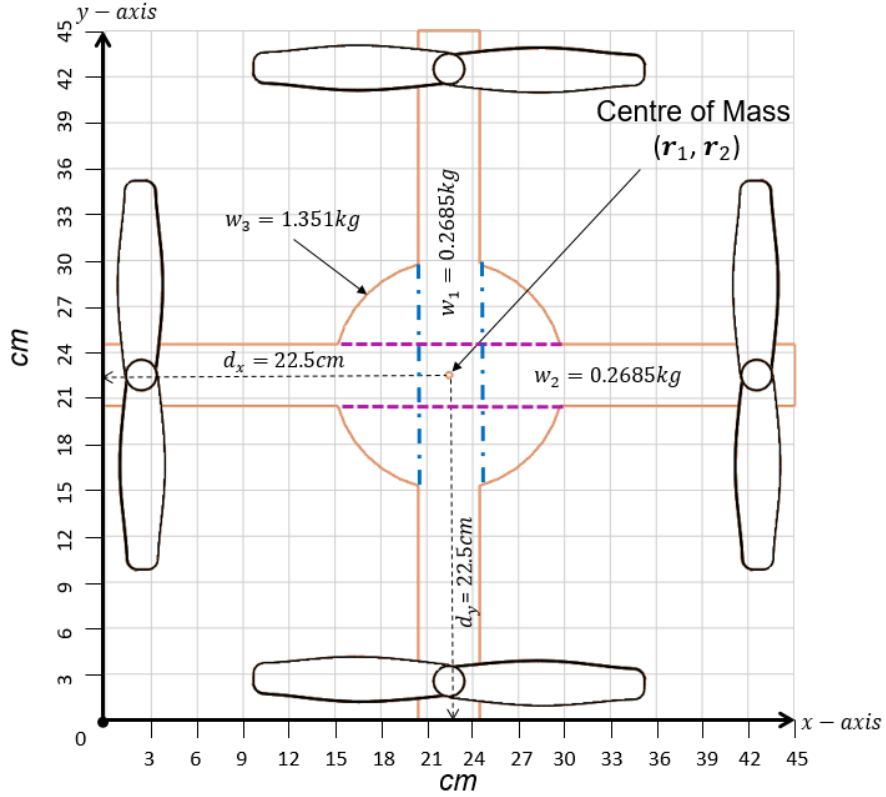
Figure 5. Top view of the Quadrotor where the COM is presented for the x and y axes.

With regards to the COM point vector along the z-axis, there are no changes to the vehicle structure which validates the fact that it will remain a constant. This can also be verified as:

$$\bar{r}_z = \frac{(w_1 \times (d_z + r_3)) + (w_2 \times d_z) + (w_3 \times d_z)}{w_1 + w_2 + w_3} \tag{26}$$

Where r_3 is the COM point vector for the vehicle shell, which in this case is a constant. For simplicity, figure 6 illustrates a side view of the vehicle where the COM is right at the cross section between the distances d_x and d_z.
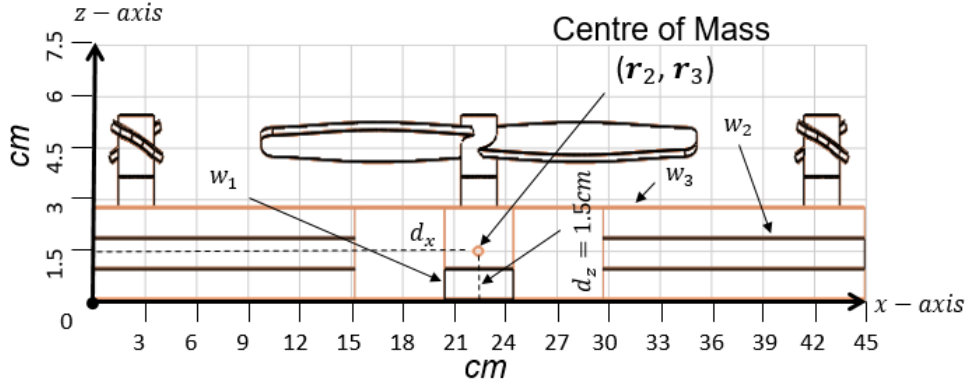
Figure 6. Side view of the Quadrotor frame illustrating the COM along the z-axis.

Once the COM changes, the MOI which is the quantity that expresses the resistance of the body angular acceleration also changes. The summation of the vehicles three mass components must be considered when mathematically determining the change in inertia as the extendable plates are displaced. Table 3 presents the MOI for each component and its relative mass, where the summation of each rotational inertia is calculated with the assumption that the extendable plates maintain their initial positions. Figure 7 explains this further where each component consists of its own relative body coordinate frame, and that the MOI determined is around that corresponding axis.

Component	Coordinate Frame	Mass	I_x	I_y	I_z
Shell	BS	$1.35 Kg$	9.9492×10^{-3}	9.9492×10^{-3}	1.9689×10^{-2}
EP1	BP1	$0.2685 Kg$	4.5388×10^{-3}	3.843×10^{-5}	4.573×10^{-3}
EP2	BP2	$0.2685 Kg$	3.843×10^{-5}	4.5388×10^{-3}	4.573×10^{-3}
Total	-	$\mathbf{1.888 Kg}$	$\mathbf{1.453 \times 10^{-2}}$	$\mathbf{1.453 \times 10^{-2}}$	$\mathbf{2.884 \times 10^{-2}}$

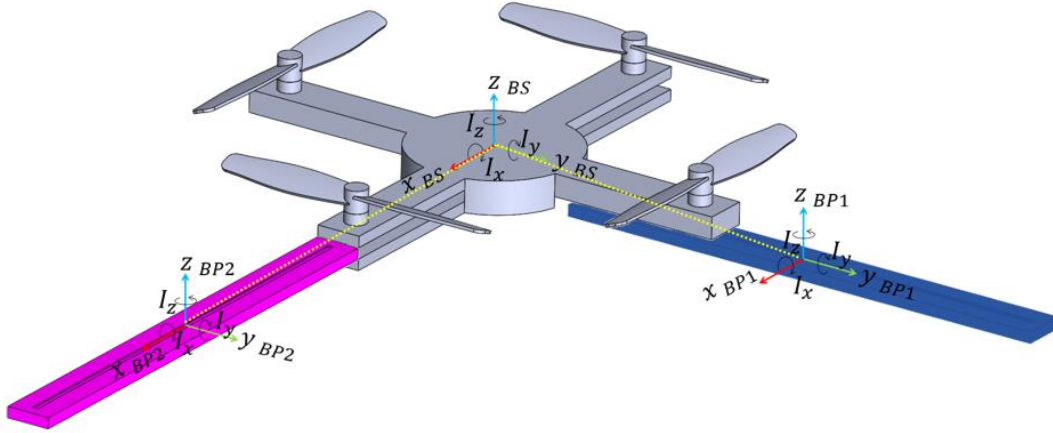Table 3. The Mass and MOI of each component

Figure 7. The coordinate frame is placed at the COM for each component.

While the MOI presented in table 3 assumes that the vehicle structure remains unchanged, any displacement of either EP1 or EP2 will generate new variables about the relative axis, which is calculated as:

$$I_{x_v} = \left(\boldsymbol{r_1}^2 \times w_1\right) + I_{xx} \tag{27}$$

$$I_{y_v} = \left(\boldsymbol{r_2}^2 \times w_2\right) + I_{yy} \tag{28}$$

$$I_{z_v} = \left(\boldsymbol{r_1}^2 \times w_1\right) + \left(\boldsymbol{r_2}^2 \times w_2\right) + I_{zz} \tag{29}$$

Where I_{x_v}, I_{y_v} and I_{z_v} are the new MOI variables that are effected based on the COM point vector $\boldsymbol{r_1}$ and $\boldsymbol{r_2}$ respectively. The torque generated significantly relies on the distance between the force points (i.e. propeller thrust) to the COM. In equation (20) and (21), the length l determines the torque required to rotate the vehicle. Therefore, the distance between each motor to the COM must equal the total distance between the two opposite motors. The distance l_i $(i = 1, 2)$ is determined using Pythagoras theorem:

$$l_i = \sqrt{d_h^2 + d_v^2} \tag{30}$$

Where d_h $(h = 1, 2)$ and d_v are the respective adjacent and opposite lengths as shown on figure 8. Since d_h is purely a horizontal length between the motor to the COM, it automatically becomes a variable when the plates are extended. On the

other hand, d_v is purely a constant because there are no changes to the point where the force is generated.
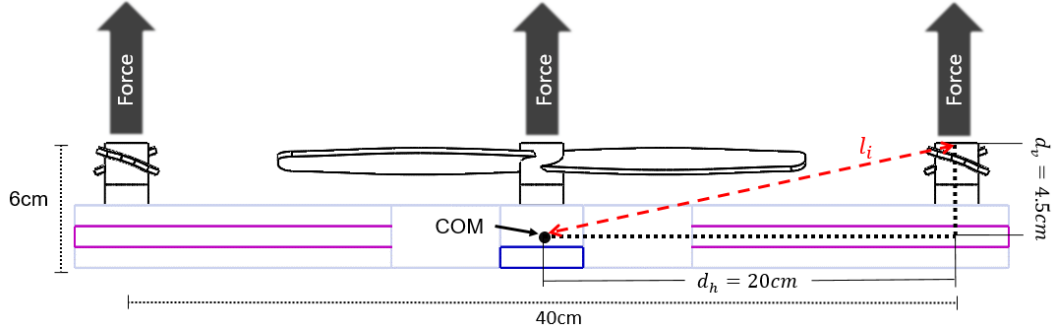

Figure 8. Calculating the length between the motor to the COM (assuming both extendable plates are at their initial positions).

Once l_i is determined for each motor respectively, the total distance D_T ($T = 1, 2$) between the two opposite motors can be calculated, where the summation of both opposite lengths is appropriately added. This concept is followed to ensure that the torque generated is accurate as the COM changes. Therefore, U_2 and U_3 presented in equation (14) are rewritten in order for the dynamic system to consider these effects:

$$U_{2v} = \left[-b\Omega_2^2 \times (D_1 - l_1) + b\Omega_4^2 \times l_1 \right] \tag{31}$$

$$U_{3v} = \left[-b\Omega_1^2 \times (D_2 - l_2) + b\Omega_3^2 \times l_2 \right] \tag{32}$$

As a result, equation (20) to (22) are now transposed to consider the changes in these variables as the extendable plates are displaced.

$$\ddot{\phi} = \frac{1}{I_{xv}} [\dot{\theta}\dot{\psi}(I_{zv} - I_{yv}) - J_r\dot{\theta}\Omega + U_{2v}] \tag{33}$$

$$\ddot{\theta} = \frac{1}{I_{yv}} [\dot{\phi}\dot{\psi}(I_{xv} - I_{zv}) + J_r\dot{\phi}\Omega + U_{3v}] \tag{34}$$

$$\ddot{\psi} = \frac{1}{I_{zv}} [\dot{\phi}\dot{\theta}(I_{yv} - I_{xv}) + U_4] \tag{35}$$

As mentioned previously, it is assumed that a force is generated from suitable actuators which drives the position of each extendable plate. In this case, U_{EP_1} and U_{EP_2} symbolises the respective forces of each plate as:

$$E\ddot{P}_1 = \frac{U_{EP_1}}{w_1} \qquad (36)$$

$$E\ddot{P}_2 = \frac{U_{EP_2}}{w_2} \qquad (37)$$

Where $E\ddot{P}_1$ and $E\ddot{P}_2$ are the accelerations for EP1 and EP2 respectively.

5. PID Controller Design

PID controllers have received a great interest from researchers due to their ease of design, tuning and reliability [47]. For this particular study, the UAV will be assessed under the influence of zero external disturbances to assess the concept of the proposed structure. Four desired inputs are considered; altitude, x-axis, y-axis and heading angles. Therefore, multiple PID controllers will be implemented where each one is set to control the six degrees of freedom respectively. This is generally referred in the literature as the whole-double loop control system which consists of; the inner-loop (attitude) and the outer-loop (position) control [48,49]. The control loop for the altitude positon can be written as:

$$U_{1c} = K_{pz}\, e_z + K_{iz}\int e_z dt + K_{dz}\, \dot{e}_z \qquad (38)$$

Further expanding equation (39) gives:

$$U_{1c} = K_{pz}(z_d - z) + K_{iz}\int (z_d - z)dt + K_{dz}(\dot{z}_d - \dot{z}) \qquad (39)$$

Similarly, the inner-loop control for roll, pitch and yaw is expressed as:

$$U_{2c} = K_{p\phi}(\phi_d - \phi) + K_{i\phi}\int (\phi_d - \phi)dt + K_{d\phi}(\dot{\phi}_d - \dot{\phi}) \qquad (40)$$

$$U_{3c} = K_{p\theta}(\theta_d - \theta) + K_{i\theta} \int (\theta_d - \theta)dt + K_{d\theta}(\dot{\theta}_d - \dot{\theta}) \tag{41}$$

$$U_{4c} = K_{p\psi}(\psi_d - \psi) + K_{i\psi} \int (\psi_d - \psi)dt + K_{d\psi}(\dot{\psi}_d - \dot{\psi}) \tag{42}$$

Where the reference angles used to represent the roll, pitch and yaw respectively are ϕ_d, θ_d and ψ_d.

While the controllers presented in equation (39) to (42) can enforce successful tracking for the altitude and rotational angles, reaching the desired positions along the horizontal positions is impractical in this stage. Therefore, researchers have discovered a position tracking approach by introducing more controllers to the system that function in an outer-loop manner. Figure 9 explains this further where the outer-loop corresponds to the input of the inner-loop control system in order to achieve the desired positions [50,51].
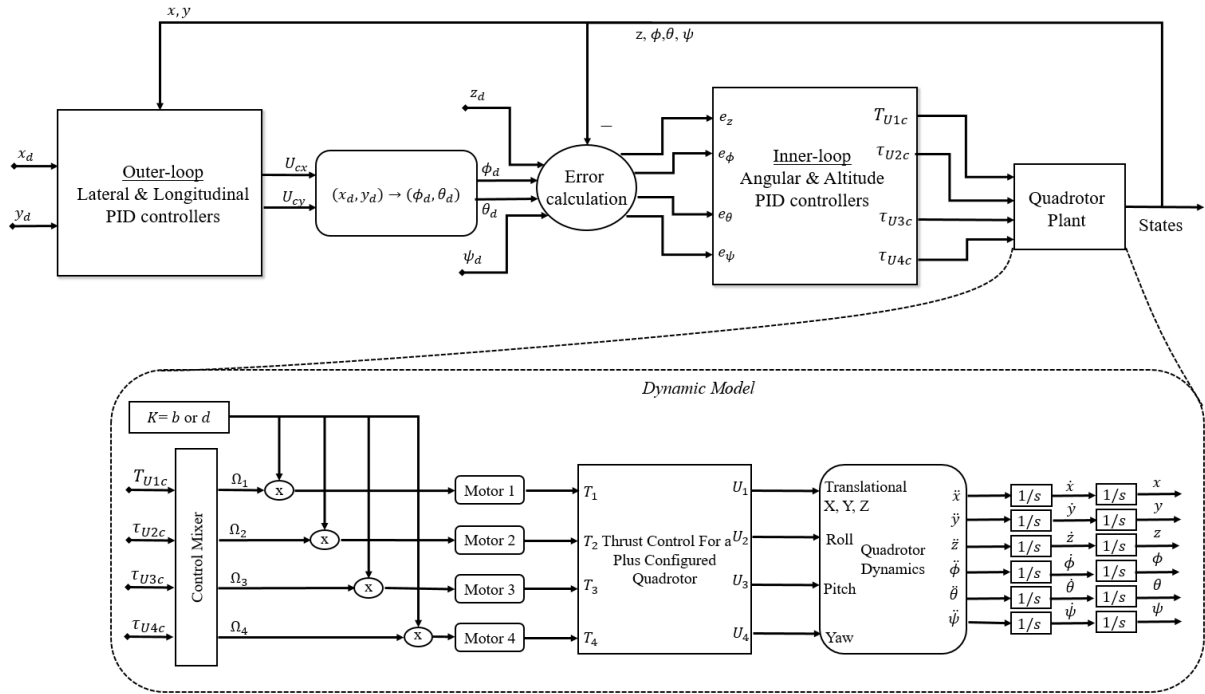

Figure 9. Whole-double loop control architecture.

Essentially, the position controllers will generate a signal that will act as an input to θ_d and ϕ_d correspondingly. To find the link between the generated controls from the outer-loop system to the inner-loop system, the translational equations governing the accelerations for the vehicle are firstly presented [33, 50, 52, 53]:

$$m\ddot{\mathbf{r}}^{bf} = \begin{bmatrix} 0 \\ 0 \\ -mg \end{bmatrix} + \mathbb{R}_M \begin{bmatrix} 0 \\ 0 \\ U_1 \end{bmatrix} \tag{43}$$

Where $\mathbb{R}_M$ is the Euler rotational matrix and $\mathbf{r}^{bf}$ is the vehicles position with respect to the inertial frame. Expanding equation (43) further will provide the following expression:

$$m \begin{bmatrix} \ddot{x} \\ \ddot{y} \\ \ddot{z} \end{bmatrix} = \begin{bmatrix} 0 \\ 0 \\ -mg \end{bmatrix} + \begin{bmatrix} c_\psi c_\theta & c_\psi s_\theta s_\phi - c_\phi s_\psi & c_\phi s_\theta c_\psi + s_\psi s_\phi \\ c_\theta s_\psi & c_\psi c_\phi + s_\psi s_\theta s_\phi & s_\theta s_\psi c_\phi - c_\psi s_\phi \\ -s_\theta & c_\theta s_\phi & c_\theta c_\phi \end{bmatrix} \begin{bmatrix} 0 \\ 0 \\ U_1 \end{bmatrix} \tag{44}$$

As mentioned previously, the x and y position of the Quadrotor plant cannot be controlled directly using one of the four control laws (U_1, U_2, U_3, U_4). Therefore, we linearize equation (44) to get the difference in acceleration between the translational motion and the relative desired angular motion. We assume that the UAV is stable around a hovering point and that there are negligible attitude rotations; $\phi \approx 0, \theta \approx 0, \dot{\phi} \approx 0, \dot{\theta} \approx 0$. Hence, simplifying equation (44) is expressed as:

$$U_{cy} = g(cos\psi + sin\psi) \tag{45}$$
$$U_{cx} = g(sin\psi - cos\psi) \tag{46}$$

Where U_{cx} and U_{cy} are the acceleration control output along the x and y-axis respectively. Expressing equation (45) and (46) in a matrix form and including the desired angles that are coupled with the relative translational position is presented as:

$$\begin{bmatrix} U_{cy} \\ U_{cx} \end{bmatrix} = g \begin{bmatrix} cos\psi & sin\psi \\ sin\psi & -cos\psi \end{bmatrix} \begin{bmatrix} \phi_d \\ \theta_d \end{bmatrix} \tag{47}$$

Applying the inverse matrix and rearranging the formula to make the desired attitude the subject is:

$$\begin{bmatrix} \phi_d \\ \theta_d \end{bmatrix} = \frac{1}{g} \begin{bmatrix} sin\psi & cos\psi \\ cos\psi & -sin\psi \end{bmatrix}^{-1} \begin{bmatrix} U_{cx} \\ U_{cy} \end{bmatrix} \tag{48}$$

$$\begin{bmatrix} \phi_d \\ \theta_d \end{bmatrix} = \frac{1}{g(-sin\psi^2 - cos\psi^2)} \begin{bmatrix} -sin\psi & -cos\psi \\ -cos\psi & sin\psi \end{bmatrix} \begin{bmatrix} U_{cx} \\ U_{cy} \end{bmatrix} \tag{49}$$

The determinant of the matrix $sin\psi^2 + cos\psi^2 = 1$. Hence, equation (49) is expressed as:

$$\phi_d = \frac{1}{g}(U_{cx}sin\psi + U_{cy}cos\psi) \tag{50}$$

$$\theta_d = \frac{1}{g}(U_{cx}cos\psi - U_{cy}sin\psi) \tag{51}$$

Therefore, the mathematical representation of the x and y controllers in the outer-loop within figure 9 are given as:

$$U_{cx} = K_{px}(x_d - x) + K_{ix}\int(x_d - x)dt + K_{dx}(\dot{x}_d - \dot{x}) \tag{52}$$

$$U_{cy} = K_{py}(y_d - y) + K_{iy}\int(y_d - y)dt + K_{dy}(\dot{y}_d - \dot{y}) \tag{53}$$

Where x_d and y_d are the desired positions of the UAV respectively. Finally, controlling the positional displacement of $EP1$ and $EP2$ is achieved through a direct force generated by simple PID techniques.

$$U_{EP1} = K_{P1}(EP1_d - EP1) + K_{i1}\int(EP1_d - EP1)dt + K_{d1}(E\dot{P}1_d - E\dot{P}1) \tag{54}$$

$$U_{EP2} = K_{P2}(EP2_d - EP2) + K_{i2}\int(EP2_d - EP2)dt + K_{d2}(E\dot{P}2_d - E\dot{P}2) \tag{55}$$

Where $EP1_d$ and $EP2_d$ are the desired positions and $EP1$ and $EP2$ are the actual positions of each plate respectively.

6. Simulation and Performance Assessment Methods

6.1. MATLAB/Simulink

Demonstrating the dynamic performance of a UAV is monumentally expressed by many authors as a set of mathematical equations in Simulink [4,45,53]. According to [54], designing a precise mathematical model that represents the full aerodynamic forces and the disturbances which act on the Quadrotor is challenging, and that increasing the results accuracy is essentially relied on improving the mathematical representation. Research groups in [55] have also mentioned that analysing the behaviour of more emerging vehicle structures is becoming complicated to mathematically model. This is due to the introduction of new aerodynamic challenges and the motion of moveable components within the body where the mathematical model may ignore such effects.

The method used in modelling the dynamic system is set by applying angular velocities measured in radians per second (RPS) to the four respective motors. As the motor speed is increased, the propellers generate a thrust which is summed to a total thrust as presented in equation (14). The resultant motions are then calculated based on the direct cosine matrix in equation (2). However, it is worth mentioning that this approach is used to represent the dynamics of a rigid body rather than the imagined Quadrotor, which simplifies the complexity of the practical system as a result [54,56,57].

6.2. Msc ADAMS

Msc ADAMS is an abbreviation for automatic dynamic analysis of mechanical systems, which is a calculation program that is capable of modelling and simulating almost any mechanical system. In particular, the bodies to be modelled

must be able to achieve one or more degrees of freedom. The software supports engineers in studying the dynamics of a particular body that consist of numerous moving parts (i.e. multi-body interaction) based on the loads, forces and constraints distributed within the body [58].

In the process of designing and studying complex mechanical systems, the author in [59] mentions that a number of fundamental questions are raised concerning the intended behaviour and the actual response. When the mechanics of a particular geometry involve the transfer of motions from one body to another to achieve larger rotations and translations, using a mechanical computer aided engineering software (MCAE) such as ADAMS can accurately simulates the performance of the designed product prior to practically building the prototype.

In order to obtain simulation results from ADAMS environment, each component within the geometry consists of attributes such as mass, material, moment of inertia, constraints, and drive inputs. The attributes on table 3 are configured to the relative components while fixed joints are applied between the chassis and actuators, revolute joints are applied between the propellers and their relative actuators. As for the extendable plates, a translational joint in contact with the vehicle chassis is used in order to achieve the required displacement respectively. To achieve positional tracking, the PID controllers designed in Simulink for the mathematical model will also be used in ADAMS. Therefore, both software are linked together using the co-simulation feature.

6.3. Co-simulation

By designing and developing the Quadrotor model in ADAMS, analysing the dynamic behaviour of the vehicle can be manually initiated by increasing the

angular velocity of the motors. This will generate a thrust which will enforce the vehicle to lift and rotate according to the control inputs. However, the implementation of a control algorithm can be directly implemented within the software, but ADAMS consists of a feature that allows the analyst to study the performance of the mechanical system in a more detailed manner.

Co-simulation is supported by the software which refers to the process of simulating a system with the inclusion of two or more simulation tools. A communication between both software is simultaneously carried out during run-time which provides users with the capability of analysing various aspects between both platforms [60]. In this case, a Co-simulation between ADAMS and Simulink can be carried out where, ADAMS encompasses the modelling features and constraints while Simulink is used to design the control algorithm. Figure 10 explains this further using a block diagram which consists of an overview about the functionality of this feature. Initially, the quadrotor dynamics in ADAMS presents an accurate simulation similar to a practical model where the theoretical representation is not required [61]. As the system states are generated, it is transferred into Simulink where the control algorithm can enforce the states towards the desired region.
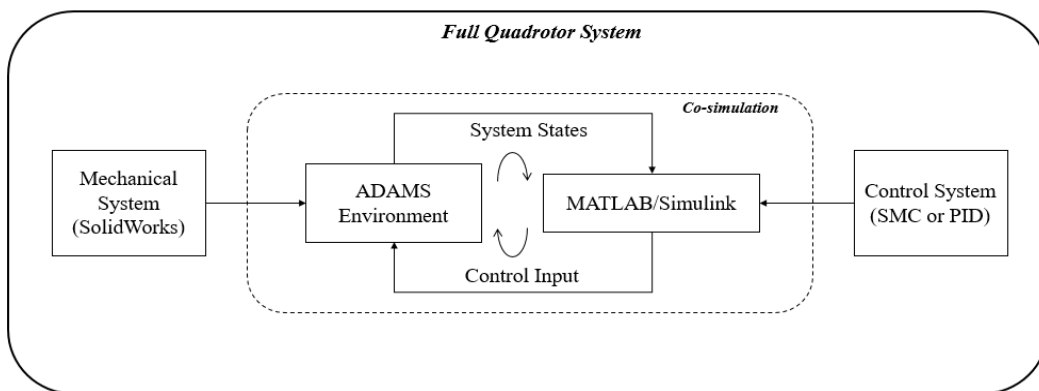

Figure 10. Co-simulation of the Quadrotor system between ADAMS and Simulink.

7. Mathematical and Physical Modelling Analysis

Essentially, the main objective of this research is to study the behaviour of the vehicle as the extendable plates are respectively displaced. During this analysis, the proposed controller is used to verify the proposed concept and ensure that it is practically realisable. Moreover, comparing ADAMS (Co-simulation) against Simulink will ensure that the mathematical representation is correctly derived. Therefore, the physical parameters and the limitations applied on both software must be identical as presented in table 4.

Variable	Description	Value	Units
g	Gravitational acceleration	9.81	ms^{-2}
l	Arm Length	0.225	m
$[F_{min},F_{max}]$	Motor thrust range	$[0,12]$	N
$[(\theta_{min},\theta_{max})(\phi_{min},\phi_{max})]$	Saturated rotation	$[(-0.6,0.6)(-0.6,0.6)]$	Rad

Table 4. UAV Physical modelling parameters

The controller outputs; U_{1c}, U_{2c}, U_{3c} and U_{4c} generated by the PID controller must be mapped to generate the required thrust for each motor. This is generally referred to as the "thrust mixers", which has also been similarly implemented by the authors in [62–64]. The corrected controller output for each actuator can be achieved by following the mixing law:

$$\begin{cases} T_1 = U_{1c} - U_{3c} - U_{4c} \\ T_2 = U_{1c} - U_{2c} + U_{4c} \\ T_3 = U_{1c} + U_{3c} - U_{4c} \\ T_4 = U_{1c} + U_{2c} + U_{4c} \end{cases} \tag{56}$$

7.1. Dynamic Analysis

In this section, the transient Quadrotor dynamics are analysed on Simulink and ADAMS without using any control techniques. Essentially, the minimum thrust required by each motor must exceed 4.63N (for a vehicle of weight 1.888kg) in

order to achieve lift. For example, Figure 11 (a) illustrates that once 5N (88.9RPS) is applied simultaneously to each motor, the vehicle has risen vertically upwards. In addition, simultaneously applying 4N (79.6RPS) to each motor indicates that; due to the gravitational force overcoming the lift force, the vehicle began to descend. Another example is also presented in figure 11 (a) where the control input for each motor is configured to synchronously oscillate between 0N to 15N. This is carried out in order to ensure that the response between both software is accurately modelled as the vehicle varies in its altitude.

Figure 11 (b) illustrates the vehicle's attitude response as the thrust (i.e. speed) of a single motor is varied. A sinusoidal control input is set to continuously change between 4.8N (71.1RPS) and 5.2N (106.7RPS) for motors 1 and 2 in order to evaluate the dynamics. Therefore, rolling and pitching angles are effected which caused the multirotor to horizontally move along the coupled y and x-axis respectively. By comparing ADAMS and Simulink, the results clearly indicate that the transient motions are superimposed for every study. Therefore, it can be concluded that the geometry designed and imported into the physical modelling software has successfully justified the performance of the mathematical model. Moreover, ADAMS has illustrated a 3D visual representation of the vehicle during flight while Simulink was only limited to a set of numerical results.
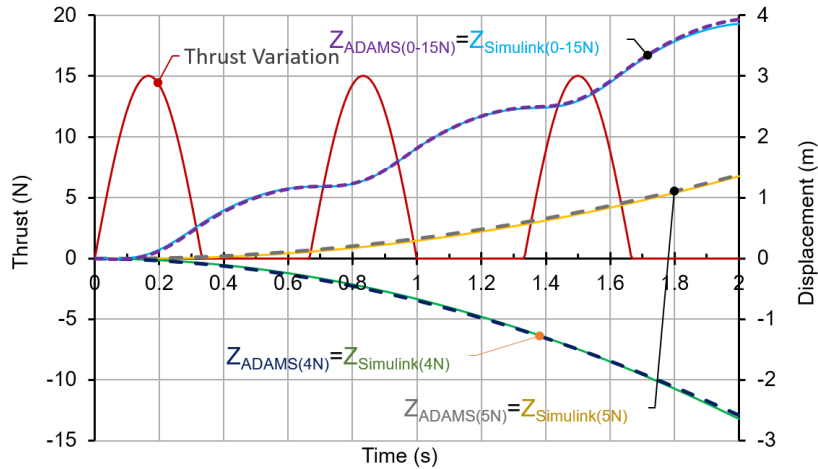
a) Simulink and ADAMS Quadrotor response to a half-wave-rectified and constant trust input
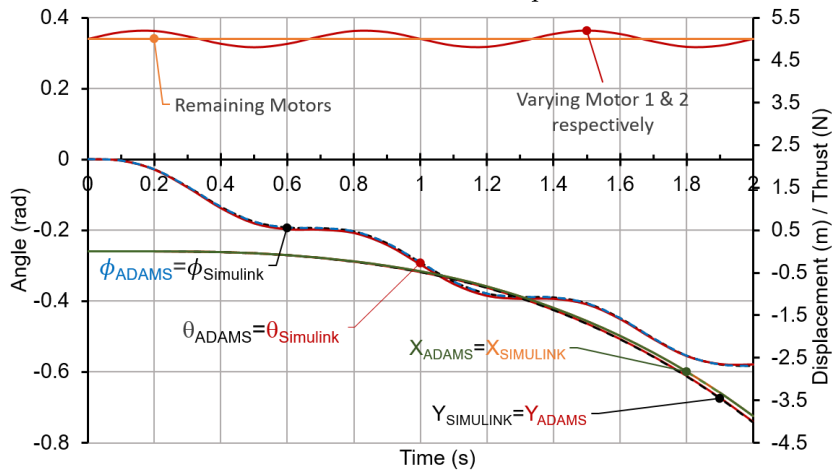
b) Varying thrusts for Motor 1 and Motor 2 between 4.8N and 5.2N respectively using Simulink and ADAMS.

Figure 11. Applying constant and variable thrusts to the Quadrotor while Simulink and ADAMS are compared.

7.2. *Structural Variation Impact on Flight Performance*

This section focuses on the implementation of PID controllers similar to the block diagram presented in figure 9. The control system was first tested and validated following several simulations where trial and error approach was used to determine the most appropriate gains. These are:

Controller	P	I	D
Altitude, z	10.1	0.01	7.5
Rolling, ϕ	5.5	0.01	1.1
Pitching, θ	5.5	0.01	1.1
Yawing, ψ	4.2	0.01	0.8
Lateral, x	3.9	0.001	4.3
Longitudinal, y	3.9	0.001	4.3
EP1	22	0	4.1
EP2	22	0	4.1

Table 5. PID parameters selected for each controller

7.2.1. *Extendable Plates Analysis*

Upon selecting the parameter gains for each controller, the extendable plates were displaced while the vehicle maintained a hovering altitude. During this assessment, the desired rotational angles for rolling, pitching and yawing were all set to zero. Figure 12 illustrates the analysis undertaken for the extendable plate, where the Quadrotor dynamics are thoroughly studied. Iterative simulations where carried out with a displacement starting initially from 1cm and moving up to 15cm. While the reference positions where identically applied for ADAMS and Simulink, the transient response between both signals illustrates that there is a slight difference during the early stages of reaching the reference position (below 1s). As the vehicle progresses into settling at the desired position, both signals become superimposed.
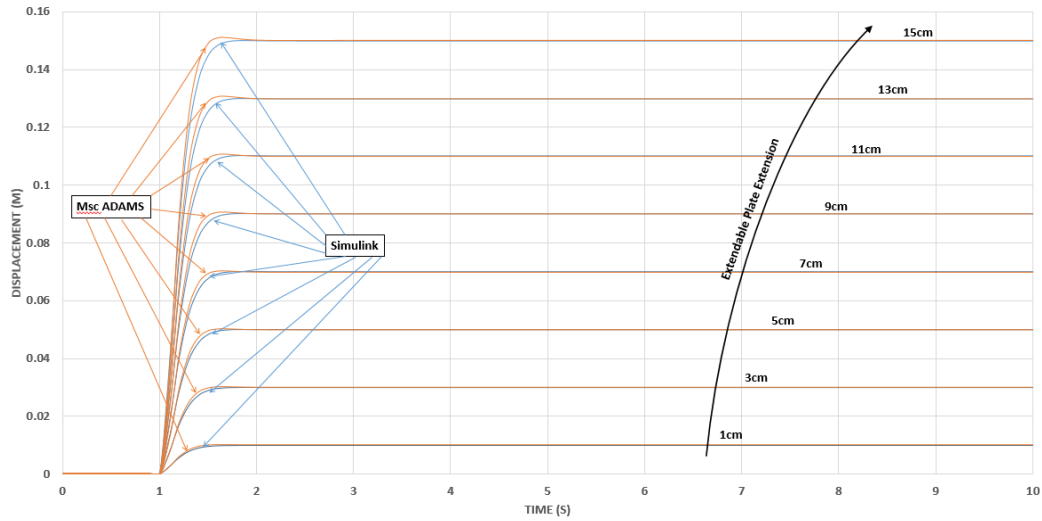
Figure 12. The positional displacement of each extendable plate from 1cm up to 15cm.

During the transition of each extension, the dynamic behaviour will be focused on attaining the effected rotational and translational motions. Figure 13 (a) presents the vehicle motion along the y-axis and the effected rotational angles as EP1 is displaced. A related point to consider is that the extension of the corresponding plate will effect a rotational angle which is coupled with a relative translational position. For instance, extending EP1 by 15cm will effect roll by 0.177 Radians (10.1° approx.) in which the translational behaviour along the y-axis moved by approximately 53 meters within a 9s margin.

Similarly, figure 13 (b) illustrates the dynamic changes on ADAMS with identical inputs to the Simulink model shown in figure 13 (a). A comparison between both software illustrates that the transient behaviour is fairly identical with marginal differences. For instance, extending EP1 by 15cm effected the rolling angle by 0.182 radians (10.4° approx.) in which the translation motion along the y-axis reaches approximately 54 meters within a 9s margin. By analysing both graphs, the resultant translational motion is very similar because both physical components consist of the same mass as well as the MOI.
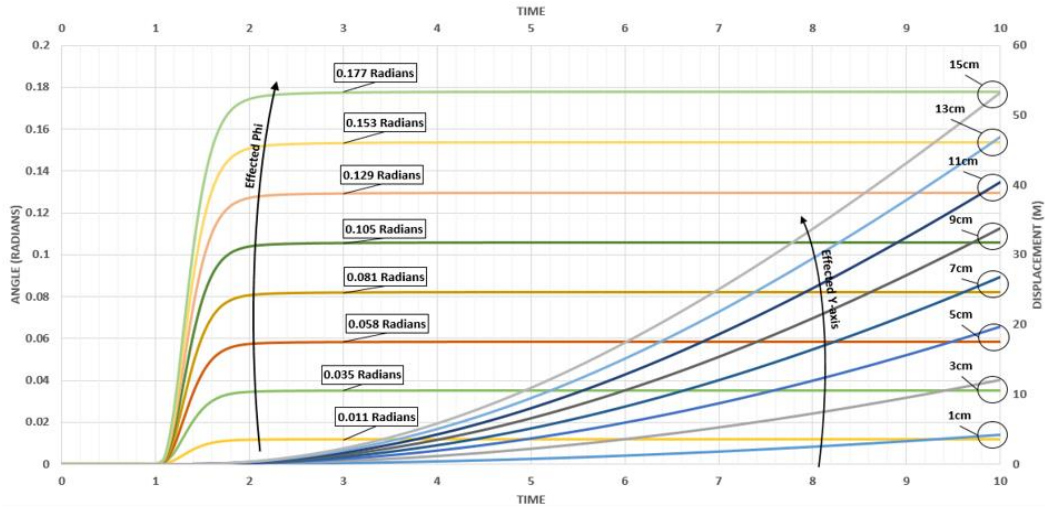
a) Translational y-axis motion and coupled roll (phi) angle due to EP1 on Simulink
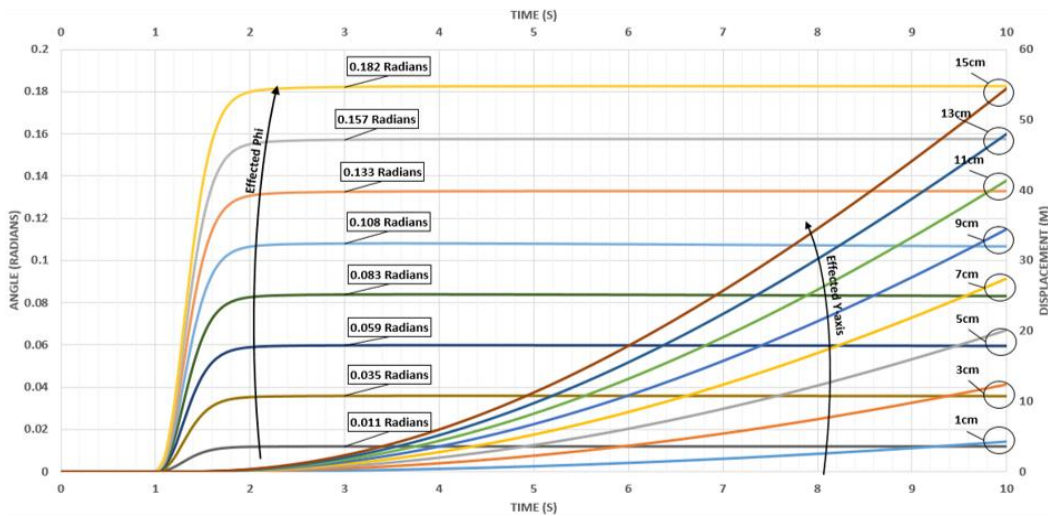
b) Translational y-axis motion and coupled roll (phi) angle due to EP1 on ADAMS

Figure 13. Extending EP1 effected the rotational and translational motions from hovering conditions.

Clearly, increasing the displacement of the plates at different iterations indicates that the effected rotation is also increased. These effects only occur due to the structural changes of the vehicle, where a hovering position would be maintained if the structure does not change. Hence, it can be concluded that displacing EP1 will alter the rolling angle and effect the y-axis, while displacing EP2 will alter the pitching angle and effect the x-axis. Moreover, the maximum displacement which is set to 15cm causes the vehicle to rotate by up to 0.177 radians on Simulink and 0.182 radians on ADAMS from a hovering position. As for yawing, the system

states have presented no effects where it is believed that the proposed mechanical system is only capable of enforcing the vehicle to roll or pitch according to the relative structural changes.

In order to verify the performance further, Figure 14 illustrates how the vehicle performed as EP1 and EP2 are displaced simultaneously by 10cm. Maintaining a hovering position and applying the desired displacement at 1s caused the vehicle to rotate in both angles simultaneously, which also enforced motions along the x and y-axis in a transient form. While the vehicle continues to uphold a specific structure during flight, the positional motion along the horizontal axes will continue to infinitely rise over time so long as the rotational angles are not zero. Hence, figure 14 indicates that the translational motion is continuously rising with EP1 and EP2 extended. Moreover, applying an identical displacement of the extendable plates on both software illustrates that ADAMS has reached an increased rotational angle of approximately 0.1 degrees in comparison to Simulink. Therefore, the final position reached at 10s is 0.8 meters higher than Simulink.
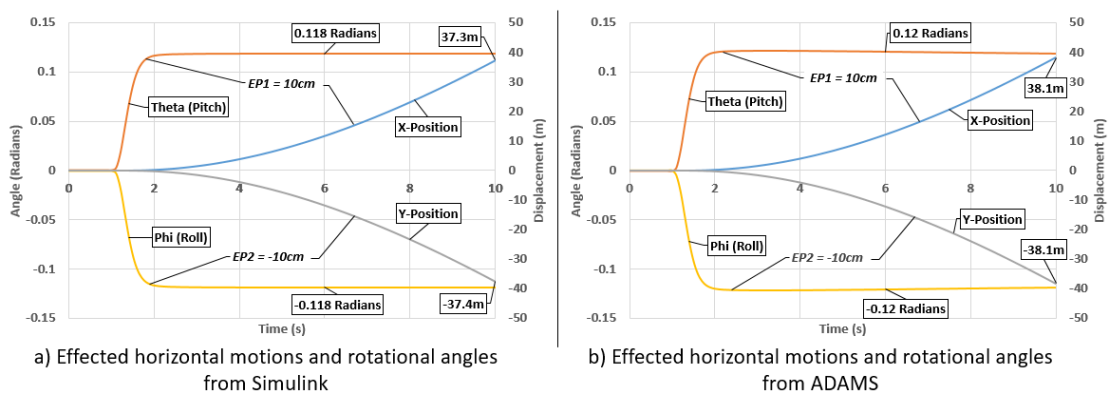

a) Effected horizontal motions and rotational angles from Simulink

b) Effected horizontal motions and rotational angles from ADAMS

Figure 14. Simultaneously extending EP1 and EP2 by 10cm while hovering.

7.2.2. *Changing Structure during Rotation*

To study the performance of the novel structure further, the vehicle is set to carry out a desired rotational angle of 0.6 radians (34° approx.) at the 1s interval.

Figure 15 (a) presents the resultant motion along the y-axis where the final position reached is 151.9 meters at 10s while maintaining EP1 and EP2 at their initial positions. On the other hand, a separate response is presented along the same axis where the final position reached is 180.9 meters due to the extension of EP1 by 14cm. Finally, Figure 15 (a) also illustrates a separate response of the Quadrotor where 133.5 meters is reached when the extension of EP1 is displaced along the opposite direction by 14cm.

Figure 15 (b) is coupled with the translational motion in figure 15 (a) where the vehicle maintained zero steady state error once the desired angle is reached. This is purely set on studying the behaviour similar to a traditional Quadrotor while upholding the positions of EP1 and EP2 at their initial positions. By repeating the simulation, EP1 was extended at 4s by 14cm in the positive direction which caused the vehicle to reach a higher position by approximately 29 meters in comparison to the traditional version (without EP1 & EP2 extension). The desired angle between 1s to 4s is accurately tracked until EP1 is displaced, which has caused the vehicle to further rotate by approximately 0.24 radians (14° approx.). Then, repeating the simulation and extending EP1 in the opposite direction caused the Quadrotor to deviate away from the desired angle by 0.18 radians (10° approx.). As a result, the final position reached was reduced by approximately 18.4 meters which is due to the mass distributed along the body moving to the opposite side of which the vehicle is turning.

As for figure 15 (c) and figure 15 (d), reference inputs where applied on ADAMS which were identical to the Simulink model. Clearly, there is a marginal difference in relation to the final positions reached. While upholding EP1 and EP2

at their initial positions, Simulink presented an increased position of 5.27% in comparison to ADAMS. As for displacing EP1 to increase the vehicle rotation, Simulink presented a 0.56% increased final position in comparison to ADAMS. Finally, extending EP1 in the opposite direction is 2.38% different in Simulink compared to ADAMS.

The resultant motions indicates that the performance derived can be a useful methodology in increasing the rotational boundary as compared to the traditional version. For instance, assuming that the Quadrotor is carrying out missions that require quick translational or attitude motions, the displacement of EP1 or EP2 can be a useful approach in improving the vehicles performance. Moreover, displacing any of EP1 or EP2 along the opposite direction of which the vehicle is turning, will reduce the rotational angle towards the hovering region.
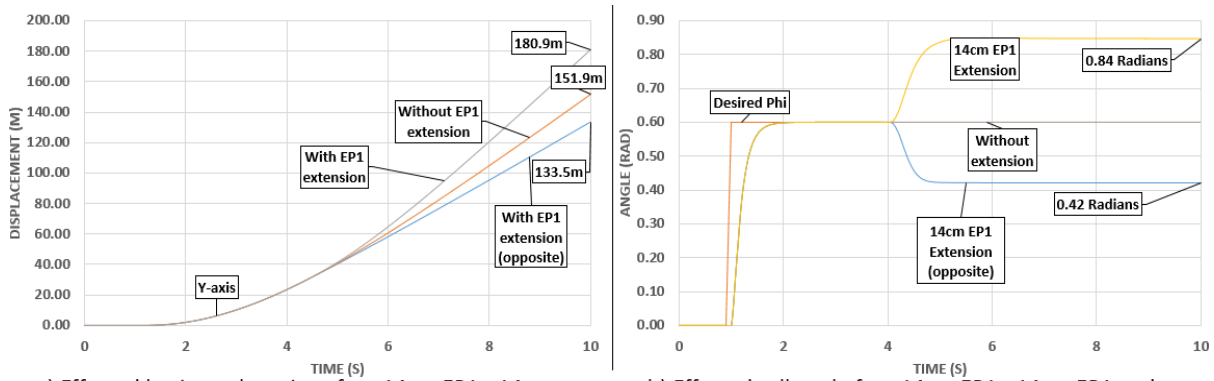
a) Effected horizontal motions for +14cm EP1, -14cm EP1 and no EP1 extension from Simulink

b) Effected roll angle for +14cm EP1, -14cm EP1 and no EP1 extension from Simulink
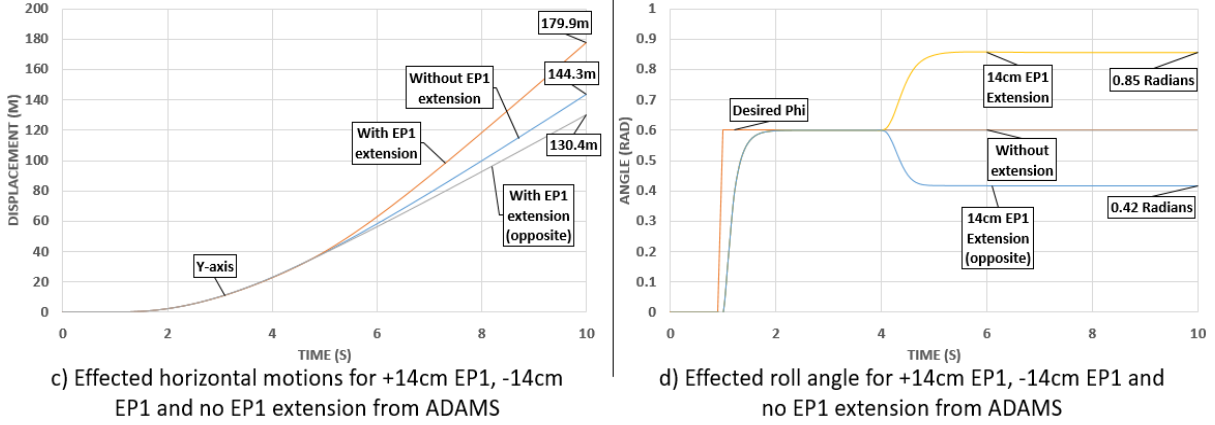
c) Effected horizontal motions for +14cm EP1, -14cm EP1 and no EP1 extension from ADAMS

d) Effected roll angle for +14cm EP1, -14cm EP1 and no EP1 extension from ADAMS

Figure 15. Extending EP1 in opposite directions at 4s while the vehicle is tracking the desired rotational angle of 0.6 radians.

7.2.3. *Improved Position Tracking*

Stabilisation and position tracking are currently used within many applications for autonomous flying. Here, the study focuses on analysing the effects of the Quadrotor as the structure changes during flight. Previous assessments has illustrated that the attitude response can change based on altering the Quadrotor structure. In this particular study, initiating the desired position along a particular axis while extending the relative plate will be analysed and compared against the traditional version (without extension). In order to correlate the angular momentum with the extendable plates, equation (57) and (58) are presented which focus on retracting the plates based on the relative rotational angle.

$$\frac{\phi_{lim} \times EP1_{max}}{\phi_{lim+}} = EP1_d \tag{57}$$

$$\frac{\theta_{lim} \times EP2_{max}}{\theta_{lim+}} = EP2_d \tag{58}$$

Where ϕ_{lim}, θ_{lim} represents the systems states which are bounded to $0.6\ Rad < \phi_{lim}, \theta_{lim} > -0.6\ Rad$, $EP1_{max}$ and $EP2_{max}$ are constants that represent the maximum displacement of 13cm to ensure stability. ϕ_{lim+} and θ_{lim+} define the maximum rotations of $0.6\ Rad$.

In figure 16, the vehicle is set to reach a desired position of 400 meters along the y-axis. This simulation is carried out during hover where in figure 16 (a), the desired position is initiated at 1s. Two sets of transient curves are presented; the first one consists of reaching the final positon without the use of EP1 extension, while the second one presented a faster dynamic response by approximately 4s as EP1 is used.

Figure 16 (b) illustrates the coupled rotational angles which autonomously occurred during the reaching stage. Two sets of rotational angles are presented where one considers EP1 extension while the other upholds EP1 at the initial position. Clearly, extending EP1 to support the vehicles performance has enforced the Quadrotor to further rotate by approximately 0.22 radians (13° approx.). Additionally, as the vehicle approached the desired position at approximately 20.7s and 16.9s, marginal oscillations occurred before stabilising at the final position. Therefore, it can be concluded that the proposed changes of MOI and the COM due to EP1 can in fact support the vehicle in reaching the final positions at a faster pace without effecting the overall stability of the system.

As for figure 16 (c) and figure 16 (d), identical reference inputs were applied on ADAMS, where the dynamic behaviour is also marginally different for this particular study. By increasing the responsivity of the Quadrotor using EP1, ADAMS reached the final positon 0.1s faster than Simulink although it is approximatley 1s slower than the Simulink results (without extension).

a) Reaching desired y position with and without EP1 extension on Simulink

b) Reaching desired Roll angle with and without EP1 extension on Simulink

c) Reaching desired y position with and without EP1 extension on ADAMS

d) Reaching desired Roll angle with and without EP1 extension on ADAMS
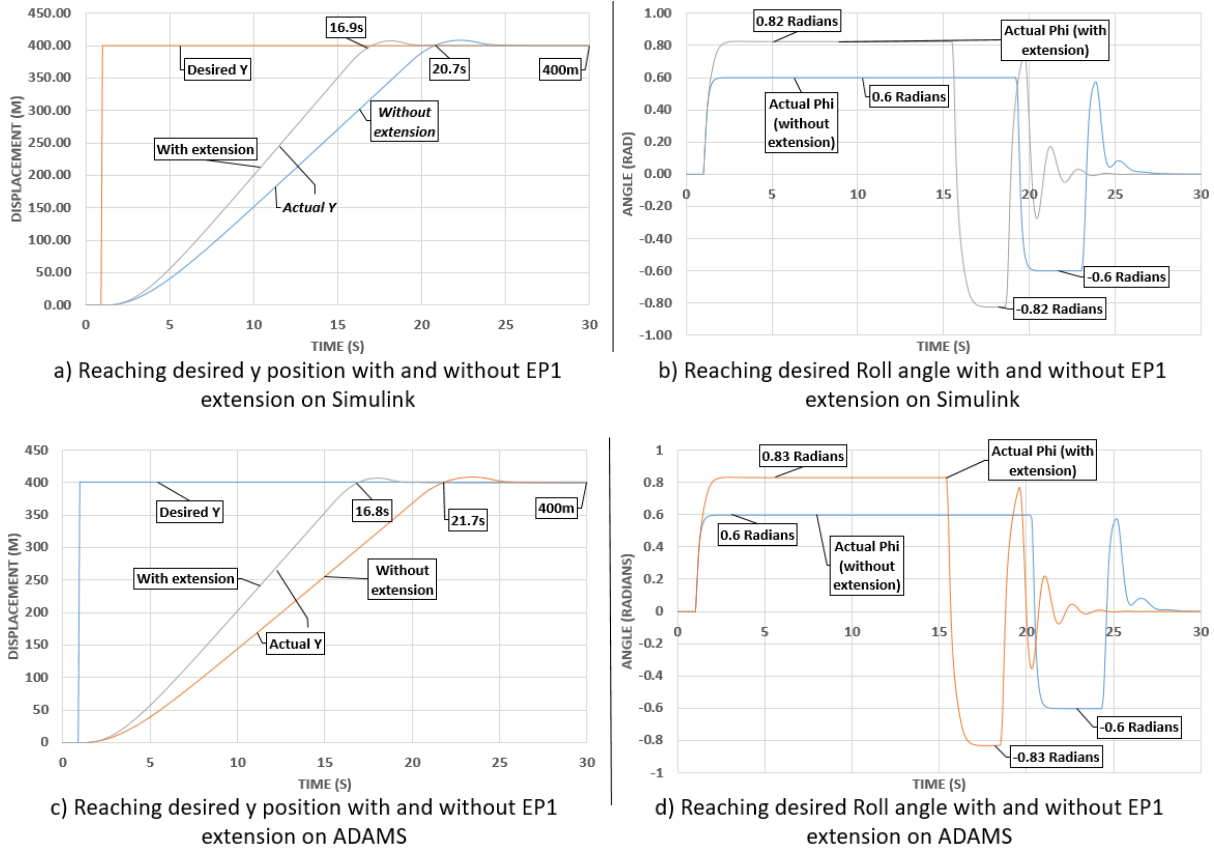
Figure 16. A comparison between the responsivity of a traditional Quadrotor (without extension) and novel Quadrotor (with extension) using PID controllers for position tracking.

8. Conclusion

This paper addressed a novel methodology in improving the performance of a traditional Quadrotor by modifying the mechanical characteristics during flight. The Quadrotor which is similar to any plus configuration has been split into three components for the design process. The first components consists of the propellers and actuators as well as the Quadrotor shell, while the other two consist of plates that carry the mass of the electronic components. The two plates which are referred to EP1 and EP2 are originally stationed coincident to the Quadrotor shell where the overall structure of the vehicle consists of similar characteristics and features to a traditional Quadrotor. During flight, EP1 and EP2 can move back and forth in a horizontal manner which causes the MOI and COM to change correspondingly.

Mission criteria such as positional tracking are applied for this study using simple PID techniques to verify the proposed concept. The resultant behaviour illustrates that the Quadrotor was able to reach the final position at a faster pace than the traditional model while maintaining stability. As for the controller implemented, the PID maintained stability during the transition of EP1 and EP2 from their initial positions. On the other hand, reaching larger displacement of the extendable plates illustrates that the Quadrotor was able to respond quicker, which is more viable for this particular study as the objectives are successfully reached.

Justifying the mathematical approach for the novel Quadrotor was achieved using ADAMS environment due to its high accuracy in modelling the dynamics of advanced mechanical systems. A comparative study was carried out between Simulink and the geometry imported into ADAMS with the inclusion of identical parameters. Initiating the desired inputs on ADAMS as well as Simulink presented a similar transient curves for all the studies carried out with marginal differences.

Therefore, we conclude that the proposed Quadrotor with the mechanical modifications has indeed presented an improved performance in comparison to the traditional version. Future contributions to this work will continue to carry out detailed dynamic analysis using physical modelling tools while using more robust control techniques. The work will also continue to simulate and analyse the dynamic behaviour of the vehicle under the presence of external disturbances.

second supervisor, Dr Mohammad Salami for his continuous support within his area of expertise.

Funding

References

[1]   M. Hassanalian, A.A.-P. in A. Sciences, Classifications, applications, and design challenges of drones: A review, Elsevier. (2017). https://www.sciencedirect.com/science/article/pii/S0376042116301348 (accessed November 17, 2020).

[2]   S. Norouzi Ghazbi, Y. Aghli, M. Alimohammadi, A.A. Akbari, Quadrotors unmanned aerial vehicles: A review, Int. J. Smart Sens. Intell. Syst. 9 (2016) 309–333. https://doi.org/10.21307/ijssis-2017-872.

[3]   J. Xiong, G.Z.-I. Transactions, Global fast dynamic terminal sliding mode control for a quadrotor UAV, Elsevier. (2017). https://www.sciencedirect.com/science/article/pii/S0019057816303627 (accessed November 17, 2020).

[4]   S. Abdelhay, A.Z.-P. Manufacturing, Modeling of a Quadcopter Trajectory Tracking System Using PID Controller, Elsevier. (2019). https://www.sciencedirect.com/science/article/pii/S2351978919302884 (accessed November 17, 2020).

[5]   A.H. Zaeri, A. Esmaeilian-Marnani, S. Bahari, M. Noor, Sliding Mode Control Improvement by using Model Predictive, Fuzzy Logic, and Integral Augmented Techniques for a Quadrotor Helicopter Model, 2019. http://mjee.iaumajlesi.ac.ir/index/index.php/ee/article/view/3155 (accessed November 17, 2020).

[6]   M. Vahdanipour, M.K. Technology, Adaptive fractional order sliding mode control for a quadrotor with a varying load, Aerosp. Sci. Technol. (2019). https://www.sciencedirect.com/science/article/pii/S1270963818318911?casa_t oken=xzqoCnfZoEwAAAAA:cW9RV8ndAoYB4PquAKHeRPSI0INcuYcaRK gLQ7X7tYaKD_5w5_iVe8ykBbwQfN8mAXHyzQ7x (accessed December 22, 2020).

[7]   S. Ariyibi, O.T. Technology, Quaternion-based nonlinear attitude control of quadrotor formations carrying a slung load, Aerosp. Sci. Technol. (2020). https://www.sciencedirect.com/science/article/pii/S1270963820306775?casa_t oken=gyv2oNILbj8AAAAA:N46Hu_sIbhpx3FswOA5NlDgAVXV_cBDnMX MxD-R9JbpuEz7KblePKQeweBSxkqkr-vSxHooe (accessed December 22, 2020).

[8]   N. Raj, R. Banavar, Abhishek, M. Kothari, Attitude control of novel tail sitter: Swiveling biplane–quadrotor, J. Guid. Control. Dyn. 43 (2020) 599–607.

https://doi.org/10.2514/1.G004697.

[9] Y. Wang, Y. Zhou, C Lin, Modeling and control for the mode transition of a novel tilt-wing UAV, Aerosp. Sci. Technol. (2019). https://www.sciencedirect.com/science/article/pii/S1270963818324684 (accessed December 22, 2020).

[10] P. Panagiotou, K.Y. Technology, Aerodynamic efficiency and performance enhancement of fixed-wing UAVs, Aerosp. Sci. Technol. (2019). https://www.sciencedirect.com/science/article/pii/S1270963818324490?casa_t oken=uXDmno1a2w0AAAAA:fUpnRYLKBweQlEw6A9Mhpr0fyv69ipTqGF N4ibSvjjUY2yr8o-1ZJkToV49keeUduv_hBUL9 (accessed December 22, 2020).

[11] A. Saeed, A. Younes, C. Cai, G.C.-P. in A. Sciences, A survey of hybrid unmanned aerial vehicles, Elsevier. (2018). https://www.sciencedirect.com/science/article/pii/S0376042117302233 (accessed November 17, 2020).

[12] A. Bin Junaid, A.D.D.C.S.- Robotics, Design and implementation of a dual-axis tilting quadcopter, Mdpi.com. (2018). https://www.mdpi.com/2218-6581/7/4/65 (accessed November 17, 2020).

[13] Y. Yildiz, M. Unel, A.E. Demirel, Nonlinear hierarchical control of a quad tilt-wing UAV: An adaptive control approach, Int. J. Adapt. Control Signal Process. 31 (2017) 1245–1264. https://doi.org/10.1002/acs.2759.

[14] Y. Govdeli, S. Muzaffar, R. Raj, B Elhadidi, Unsteady aerodynamic modeling and control of pusher and tilt-rotor quadplane configurations, Aerosp. Sci. Technol. (2019). https://www.sciencedirect.com/science/article/pii/S1270963819306261 (accessed December 22, 2020).

[15] J.-P. Reddinger, K. Mcintosh, G. Student, D. Zhao, S. Mishra, Modeling and Trajectory Control of a Transitioning Quadrotor Biplane Tailsitter, 2019. https://move.rpi.edu/sites/default/files/publication-documents/VFS 2019 Modeling and Trajectory Control of a Transitioning Quadrotor Biplane Tailsitter.pdf (accessed November 17, 2020).

[16] S.S. Chauhan, J.R.R.A. Martins, Tilt-wing eVTOL takeoff trajectory optimization, J. Aircr. 57 (2020) 93–112. https://doi.org/10.2514/1.C035476.

[17] K. Kondak, M.S. robotics and A. Huber, F, Aerial manipulation robot composed of an autonomous helicopter and a 7 degrees of freedom industrial manipulator, Ieeexplore.ieee.org. (2014). https://ieeexplore.ieee.org/abstract/document/6907148/ (accessed November 17, 2020).

[18] L.O.-I. Backus, S, Design of hands for aerial manipulation: Actuator number and routing for grasping and perching, Ieeexplore.ieee.org. (2014). https://ieeexplore.ieee.org/abstract/document/6942537/ (accessed November 17, 2020).

[19] M. Zhao, K. Kawasaki, S.N.R. and Chen, Whole-body aerial manipulation by transformable multirotor with two-dimensional multilinks, Ieeexplore.ieee.org. (2017). https://ieeexplore.ieee.org/abstract/document/7989606/ (accessed November 17, 2020).

[20] A. Honglei, L. Jie, W. Jian, W. Jianwen, M. Hongxu, Backstepping-based inverse optimal attitude control of quadrotor: Regular paper, Int. J. Adv. Robot. Syst. 10 (2013). https://doi.org/10.5772/56337.

[21] Z. Li, X. Ma, Y.L.- Neurocomputing, Robust tracking control strategy for a quadrotor using RPD-SMC and RISE, Elsevier. (2019). https://www.sciencedirect.com/science/article/pii/S0925231218314164 (accessed November 17, 2020).

[22] K.S.-2018 I.C.C. (ICC), A novel quad-rotor configuration capable of attitude control through center of gravity variation, Ieeexplore.ieee.org. (2018). https://ieeexplore.ieee.org/abstract/document/8308003/ (accessed November 17, 2020).

[23] W. Liu, G. He, H. Yu, T. Li, … J.Z.-I.C. on, Review on dynamic modeling of tilt-rotor UAVs in low speed flight, Ieeexplore.ieee.org. (2018). https://ieeexplore.ieee.org/abstract/document/8664771/ (accessed November 17, 2020).

[24] I. Morar, A, I Nascu - IEEE International Conference on Automation, Quality and Testing, Robotics, Model simplification of an unmanned aerial vehicle, Ieeexplore.ieee.org.(2012).https://ieeexplore.ieee.org/abstract/document/62377 79/ (accessed November 17, 2020).

[25] M. Herrera, W. Chamorro, A.P. Gómez, O. Camacho, Sliding Mode Control: An Approach to Control a Quadrotor, Proc. - 2015 Asia-Pacific Conf. Comput. Syst. Eng. APCASE 2015. (2015) 314–319. https://doi.org/10.1109/APCASE.2015.62.

[26] Z. Hou, P. Lu, Z.T. Technology, Nonsingular terminal sliding mode control for a quadrotor UAV with a total rotor failure, Aerosp. Sci. Technol. (2019). https://www.sciencedirect.com/science/article/pii/S1270963819316414 (accessed December 22, 2020).

[27] S. Systems, A.M. Elhennawy, Dynamic Modeling and Robust Nonlinear Control of Unmanned Quadrotor Vehicle, (2018).

[28] M.K. Habib, Dynamic Modeling and Control of a Quadrotor Using Linear and Nonlinear Approaches Heba talla Mohamed Nabil ElKholy, 2014. http://dar.aucegypt.edu/handle/10526/3965 (accessed November 17, 2020).

[29] A. Neff, Linear and Non-Linear Control of a Quadrotor UAV, 2007. https://tigerprints.clemson.edu/all_theses (accessed November 17, 2020).

[30] L. Santana, … A.B.-I.S., An Open-Source Testbed for Outdoor Navigation With the AR. Drone Quadrotor, Ieeexplore.ieee.org. (2020). https://ieeexplore.ieee.org/abstract/document/9190074/ (accessed November 17, 2020).

[31] M. Lotufo, L. Colangelo, … C.P.-M.-C.E., UAV quadrotor attitude control: An ADRC-EMC combined approach, Elsevier. (2019). https://www.sciencedirect.com/science/article/pii/S0967066118305148 (accessed November 17, 2020).

[32] A.R. Partovi, A.Z.Y. Kevin, H. Lin, B.M. Chen, G. Cai, Development of a cross style quadrotor, in: AIAA Guid. Navig. Control Conf. American Institute of Aeronautics and Astronautics Inc., 2012. https://doi.org/10.2514/6.2012-4780.

[33] A. Najm, I.I.-S. and Technology, an I. Journal, Nonlinear PID controller design for a 6-DOF UAV quadrotor system, Elsevier. (2019). https://www.sciencedirect.com/science/article/pii/S2215098618318846 (accessed November 17, 2020).

[34] X. Zhang, X. Li, K. Wang, Y.L.-A. and A. Analysis, A survey of modelling and identification of quadrotor robot, Hindawi.com. (2014). https://www.hindawi.com/journals/aaa/2014/320526/abs/ (accessed November 17, 2020).

[35] B. Stevens, F. Lewis, E. Johnson, Aircraft control and simulation: dynamics, controls design, and autonomous systems, 2015. https://books.google.com/books?hl=en&lr=&id=lvhcCgAAQBAJ&oi=fnd&pg=PR11&dq=B.+Stevens,+F.+Lewis+and+E.+Johnson,+"Aircraft+control+and+simulation:+dynamics,+controls+design,+and+autonomous+systems&ots=16c0LYcztH&sig=-6cF9gTXxfxTX9m5E9h3Xt-uIfs (accessed Nov 17, 2020).

[36] D. Wells, Schaum's Outline of Lagrangian Dynamics: With a Treatment of Euler's Equations of Motion, Hamilton's Equations and Hamilton's Principle, 1967. https://scholar.google.com/scholar?hl=en&as_sdt=0%2C5&q=D.+Wells%2C+Schaum's+Outline+of+Lagrangian+Dynamics%3A+With+a+Treatment+of+Euler's+Equations+of+Motion&btnG= (accessed November 17, 2020).

[37] Z. Shulong, A. Honglei, Z. Daibing, S. Lincheng, A new feedback linearization LQR control for attitude of quadrotor, 2014 13th Int. Conf. Control Autom. Robot. Vision, ICARCV 2014. 2014 (2014) 1593–1597. https://doi.org/10.1109/ICARCV.2014.7064553.

[38] C.A. Herda, Implementation of a quadrotor unmanned aerial vehicle, 2012. http://scholarworks.csun.edu/handle/10211.2/1053 (accessed Nov 17, 2020).

[39] K. Lee, Y. Choi, J.P.-A. Sciences, Backstepping based formation control of quadrotors with the state transformation technique, Mdpi.com. (2017). https://www.mdpi.com/2076-3417/7/11/1170 (accessed November 17, 2020).

[40] A. Zulu, S. John, A Review of Control Algorithms for Autonomous Quadrotors, Open J. Appl. Sci. 4 (2014) 547–556. https://doi.org/10.4236/ojapps.2014.414053.

[41] R. Cunha, D. Cabecinhas, C. Silvestre, trajectory Tracking tracking control quadrotor vehicle Nonlinear Trajectory Control of of a Quadrotor Vehicle, (2009) 2763–2768.

[42] M. Hancer, R. Bitirgen, I. Bayezit, Designing 3-DOF Hardware-In-The-Loop Test Platform Controlling Multirotor Vehicles, 2018. https://www.sciencedirect.com/science/article/pii/S2405896318303549 (accessed November 17, 2020).

[43] P. Niermeyer, T. Raffer, F. Holzapfel, Open-Loop quadrotor flight dynamics identification in frequency domain via Closed-Loop flight testing, in: AIAA Guid. Navig. Control Conf. 2013, American Institute of Aeronautics and Astronautics Inc, AIAA, 2015. https://doi.org/10.2514/6.2015-1539.

[44] W. Johnson, Helicopter theory, Courier Corporation , 2012. https://scholar.google.com/scholar?hl=en&as_sdt=0%2C5&q=W.+Johnson%2 C+Helicopter+theory%2C+Courier+Corporation&btnG= (accessed November 17, 2020).

[45] M. Idrissi, F. Annaz, Dynamic Modelling and Analysis of a Quadrotor Based on Selected Physical Parameters, Ijmerr.com. (2020). https://doi.org/10.18178/ijmerr.9.6.784-790.

[46] M. Wang, X. Zhang, W. Tang, J.W.-A. Sciences, A structure for accurately determining the mass and center of gravity of rigid bodies, Mdpi.com. (2019). https://www.mdpi.com/2076-3417/9/12/2532 (accessed November 17, 2020).

[47] I. Sadeghzadeh, A. Mehta, Y. Zhang, Fault/damage tolerant control of a quadrotor helicopter UAV using model reference adaptive control and gain-scheduled PID, in: AIAA Guid. Navig. Control Conf. 2011, American Institute of Aeronautics and Astronautics Inc., 2011. https://doi.org/10.2514/6.2011-6716.

[48] M. Duc, T. Trong, Y.X.-2015 I. International, The quadrotor MAV system using PID control, Ieeexplore.ieee.org. (2015). https://ieeexplore.ieee.org/abstract/document/7237537/ (accessed November 17, 2020).

[49] A. Julkananusart, I.N.-I. 2015-41st Annual, Quadrotor tuning for attitude control based on double-loop PID controller using fictitious reference iterative tuning (FRIT),Ieeexplore.ieee.org.(2015).https://ieeexplore.ieee.org/abstract/document /7392862/ (accessed Nov 17,2020).

[50] A. Nagaty, S. Saeedi, C. Thibault, M. Seto, H. Li, A. Nagaty, · S Saeedi, · C Thibault, · H Li, S. Saeedi, C. Thibault, H. Li, M. Seto, Control and Navigation Framework for Quadrotor Helicopters, J Intell Robot Syst. 70 (2013) 1–12. https://doi.org/10.1007/s10846-012-9789-z.

[51] Y. Chen, Y. He, M.Z.-J. of C.S. University, Decentralized PID neural network control for a quadrotor helicopter subjected to wind disturbance, Springer. (2015). https://link.springer.com/content/pdf/10.1007/s11771-015-2507-9.pdf (accessed November 17, 2020).

[52] D. Warren Mellinger, D. Warren, Trajectory Generation and Control for Quadrotors,2012.http://repository.upenn.edu/edissertationshttp://repository.upe nn.edu/edissertations/547 (accessed November 17, 2020).

[53] H.J.- IFAC-PapersOnLine, Position and attitude control of a quadrotor UAV using super twisting sliding mode, Elsevier. (2016). https://www.sciencedirect.com/science/article/pii/S2405896316300672 (accessed November 17, 2020).

[54] H. Mo, G. Farid, Nonlinear and Adaptive Intelligent Control Techniques for Quadrotor UAV – A Survey, Asian J. Control. 21 (2019) 989–1008. https://doi.org/10.1002/asjc.1758.

[55] D. Montagnani, M. Tugnoli, F. Fonte, A. Zanotti, M. Syal, G. Droandi, MID-FIDELITY ANALYSIS OF UNSTEADY INTERACTIONAL AERODYNAMICS OF COMPLEX VTOL CONFIGURATIONS, 2019. https://re.public.polimi.it/handle/11311/1111911 (accessed November 17, 2020).

[56] H. Foudeh, P. Luk, J.W.-2019 W. On, Quadrotor System Design for a 3 DOF platform based on Iterative Learning Control, Ieeexplore.ieee.org. (2019). https://ieeexplore.ieee.org/abstract/document/8999691/ (accessed November 17, 2020).

[57] M. Wang, Attitude Control of a Quadrotor UAV: Experimental Results, 2015. https://knowledgecommons.lakeheadu.ca/handle/2453/4153 (accessed November 17, 2020).

[58] D. Hroncová, P. Sivák, I.D.-A.M. and Materials, Kinematical Analysis of Valve Mechanism Using MSC Adams/View, Trans Tech Publ. (2015). https://www.scientific.net/AMM.816.108 (accessed November 17, 2020).

[59] R.R. Ryan, ADAMS — Multibody System Analysis Software, in: Multibody Syst. Handb., Springer Berlin Heidelberg, 1990: pp. 361–402. https://doi.org/10.1007/978-3-642-50995-7_21.

[60] SJ Rao, Vehicle modeling and Adams-Simulink co-simulation with integrated continuously controlled electronic suspension (CES) and electronic stability control (ESC) models, 2009. (accessed November 17, 2020).

[61] L. Ángel, M.P. Pérez, C. Díaz-Quintero, C. Mendoza, ADAMS/MATLAB CO-SIMULATION: Dynamic Systems Analysis and Control Tool, Trans Tech Publ. (n.d.). https://doi.org/10.4028/www.scientific.net/AMM.232.527.

[62] P. Burggräf, A.R. Pérez Martínez, H. Roth, J. Wagner, Quadrotors in factory applications: design and implementation of the quadrotor's P-PID cascade control system, SN Appl. Sci. 1 (2019). https://doi.org/10.1007/s42452-019-0698-7.

[63] S. Scholarworks, K.K. Nemirsky, Simulated Annealing-Based Optimal Proportional-Integral-Derivative (PID) Controller Design: A Case Study on Nonlinear Quadcopter Dynamics, (2017). https://doi.org/10.31979/etd.gx5m-sq86.

[64] K. Büyükkabasakal, B. Fidan, A. Savran, Mixing Adaptive Fault Tolerant Control of Quadrotor UAV, Asian J. Control. 19 (2017) 1441–1454. https://doi.org/10.1002/asjc.1479.